UNIVERSITY OF GLASGOW

College of Sciences and Engineering

School of Engineering

Master of Science by Research Thesis

Solar Power Satellites

Supervisor:
Dr. Gianmarco RADICE

Candidate:
Alessandro PALMAS

ACADEMIC YEAR 2010-2011

Abstract

During energy crisis at the end of the Sixties, a new idea to exploit solar energy arose: Solar Power Satellites. These satellites need a huge surface to collect enough solar energy to be beamed on Earth by means of a microwave power transfer system. Different concepts appeared during last forty years and a lot of studies addressing the SPS economical feasibility have been published. In this work a particular concept is considered, the JAXA Reference Concept 2003. It is a formation flying SPS, composed by two reflectors and a central array panel.

The objective of the work is to study two major problems this concept presents. Due to its dimensions, the satellite orbit will suffer from important orbital perturbations and since formation flying satellites need a tight orbit control, the first task is to derive an analytical approximation to perform relative perturbed orbit propagation for formation flying satellite. This objective is pursued starting from a H. Schaub's formulation in which formation flying satellites unperturbed orbit is described by means of an approximated relation function of orbital element differences. This formulation is merged with another approach, developed in a previous work, which gives, analytically, orbital parameters variation when a perturbation acts on the spacecraft. The result is a very interesting algorithm, able to perform the assigned task with a relative error lower than 3% over one simulated orbit.

The second objective concerns structural control. It is not possible to consider these huge satellites as rigid bodies, first natural frequencies will be certainly excited during operations. So that, the second task is the study of actuator placement optimization for flexible satellites, very useful for tight pointing requirements. A FEM model is developed modeling the SPS as a frame of beams and a global controllability index α is obtained combining modal controllability and component cost analysis. The maximization of this parameter, that depends on actuators location, maximizes the system controllability, thus it is used as cost function. Skelton's algorithm (SKE), reference point in the literature, is compared with three stochastic optimizers (GA, DE and PSO). Even if SKE gives exactly the optimal configuration it is really slow. Stochastic optimizers are all definitely faster than it. On the other hand their performance in terms of success rate ranges from 25% (GA) to over 60% (PSO). There is no certainty to find the optimum with a stochastic algorithm but in case of very detailed system models SKE–like algorithms may become unfaisible. To have a flexible instrument able to compute, with high success rate, optimal actuators configuration is a major achievement since it coniugates the possibility to perform a great number of analysis in a short time with the capability to deal with detailed models.

This page intentionally left blank

Contents

This page intentionally left blank

Chapter 1

Introduction

1.1 World Energy Situation: Early Past and Present

At the end of the Sixties a major problem arose: population growth and constant increase in energy demand led to the so called 'energy crisis'. Fossil fuels were already heavily exploited and nuclear plants were quickly growing. Important studies about future energy needs started and the situation is well presented in figure 1.1, which is dated 1968 but it is still valid. After year 2000 energy needs will have to be fulfilled by some unknown source, so that international community started to think about which would be the best solution for this situation.

Beside the energy problem, another issue gained world attention, sustainable development and environmental pollution. This aspects mix influenced some thought patterns in the research for new energy sources. In that context, renewable energy became really attractive. The new philosophy was: unlimited energy with zero environmental impact. Among different proposals, one was particularly intriguing. It was formulated by Dr. Peter Glaser in 1968[9][10]: he proposed to exploit solar power which arrives near to the Earth by means of huge satellites, called Solar Power Satellites SPS. They are equipped with two basic components: a solar collector with the task of collecting solar radiation and converting it into electrical power and a microwave antenna which has to transmit power to the Earth surface by means of electromagnetic waves (see fig. 1.5) where a receiving antenna (rectenna) will collect it. This concept is particularly appealing due to a number of factors:

- it allows to collect solar energy on orbit, i.e. outside the atmosphere, where it arrives in every moment of the day, it is not absorbed by the

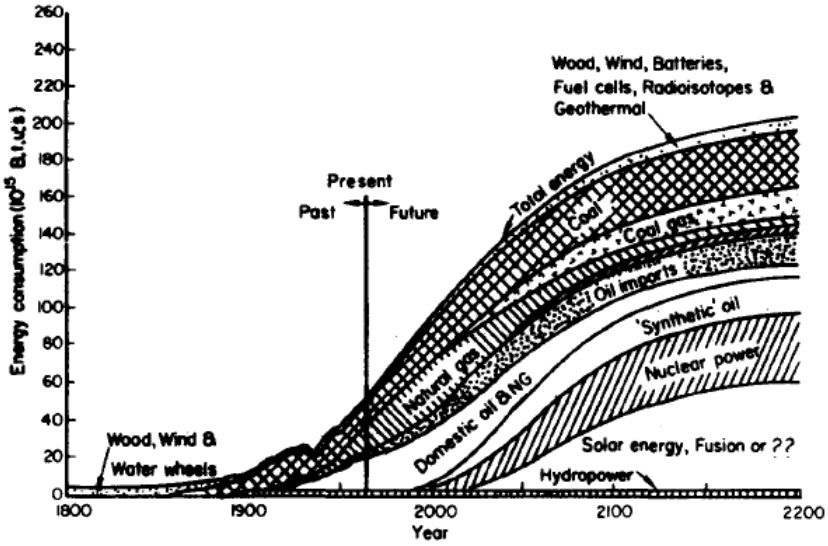

Figure 1.1: United States Energy Consumption, Year 1968

atmosphere or hidden by clouds

- it allows to limit land usage on Earth surface only for the rectenna which is smaller due to the higher power density of microwaves with respect to solar power
- if properly distributed on orbit, these satellites are able to completely fulfill world energy demand

Anyway there are also drawbacks and critical aspects

- in order to have a power production of useful amount (about $0.1-1\ GW$ of electric power) the dimensions of the satellites need to be really large (about tens of square kilometers) so that on–orbit assembly should be performed and a great number of launches would be necessary
- with a high number of launches the overall cost would increase exponentially affecting the economic feasibility
- electromagnetic wireless power transfer can be hazardous

Since their appearance, SPS have been studied under both the engineering point of view and the economic one. The latter analysis is quite important in order to evaluate if this idea is viable or not. A first, important step is to divide the energy need in categories. The energy demand daily trend varies

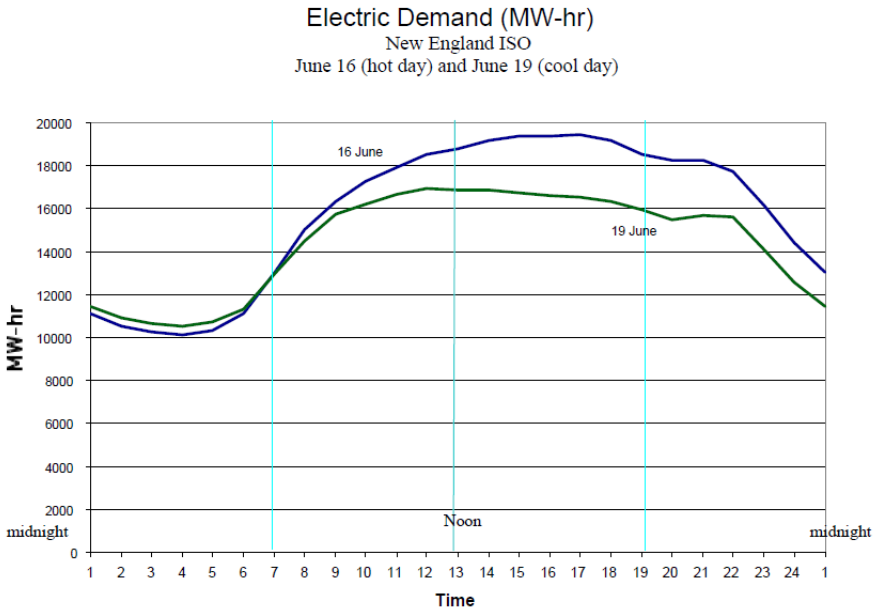

Figure 1.2: New England Typical Energy Demand Variation During 24 hours

with latitude, season and weather, but it can be in general divided in three sectors

- high demand period (see figure 1.2 between hours $10.00 - 22.00$)
- low demand period (see figure 1.2 between hours $1.00 - 10.00$ and $22.00 - 1.00$)
- peak demand (see spikes in figure 1.3)

so SPS would be used to address at least one of these needs.

High Demand Period

If SPS are employed to provide electric power in the high demand period they should

- supply energy during 12-hours/8-hours windows ($9.00-21.00$ or $10.00-18.00$) when it can be sold at higher price, so that cost–related design constraints can be relaxed
- power beam must be shared with at least 3 locations 120° Lon apart one from each other (steering system needed)

Figure 1.3: New England Typical Energy Cost Variation During 24 hours

- operational orbit can be a constellation in MEO with hand-over overlaps

Low Demand Period

In case SPS are used to face the low demand period they should be able to supply low–cost energy 24/7. This can be performed by means of

- reusable launcher: so high number of launches (about one per day) can be performed and a low cost/kg bay area (about $200 - 400$ \$/kg) could be available
- in orbit modular and automatic assembly
- lunar based production and launch
- initial investment internationally shared
- mass production components
- two choices for the operational orbit: a GEO orbit with a single SPS per ground station for constant power supply 99% time/year (very small eclipse period) or a MEO orbit constellation with a high performance electronic beam steering

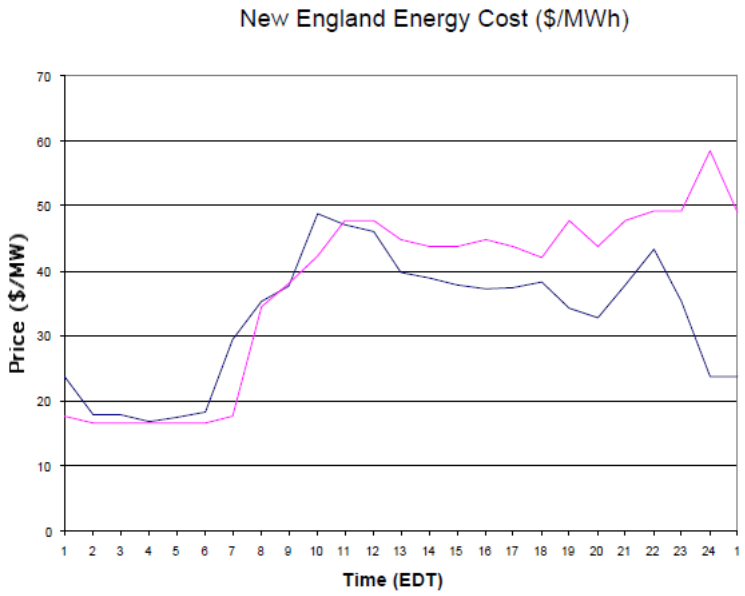

Figure 1.4: New York City Typical Energy Price Variation During 24 hours

Peak Demand

Finally, if SPS are designed to supply energy during short periods of peak demand, most important features would be

- energy beam over one location will last maximum tens of minutes when it can be sold at highest price, cost–related constraints become minor
- power beam shared with a large number of locations
- operational orbit choice can be: a GEO orbit with a wide angle and high angular rate steering system or a MEO orbit constellation with high performance steering system

All these choices should be carefully performed in order to exploit the economic return of these satellites, since the initial investment would be really relevant.

1.2 Solar Power Satellites

Since their appearance with the very first SPS concept by Peter Glaser (see fig. 1.5), a lot of different proposal arose during last forty years. NASA was the first agency to perform an accurate study on SPS, together with

Department of Energy (DOE) in 1978[25][26]. This study leads to the so called NASA-DOE SPS Reference Model (see fig. 1.6). Since then, other agencies (ESA, JAXA, etc.) and companies (Boeing[30], etc.) became interested in SPS: a lot of different concepts were proposed and different assessments[27][41][18] were performed. Hereafter some of the most important concepts are recalled and briefly described.

Peter Glaser's Concept

Glaser's concept depicted in figure 1.5, is composed by[9][10] a large circular solar collector of six kilometers of diameter and a two kilometers diameter circular antenna. The former has the task to collect and convert the solar energy into electric one, while the latter has to beam it downwards to the Earth rectenna by means of microwaves. Antenna direction is modified by means of a mechanical steering mechanism and the whole satellite is equipped with active attitude and orbit control in order to maintain the pointing accuracy. The author proposed two of these satellites in geostationary orbit with a phase between them in order to overcome the eclipse period problem; in this case the problem of shape variation due to temperature variation must be addressed. The life of the satellites is supposed to be about 30 years, the main hazard is represented by micro meteorites.

Also Sun synchronous orbits are taken into account: this particular kind of orbits takes advantage of the so called J_2 perturbation, that is an orbital perturbation caused by the asphericity of the Earth (its oblateness). It can be exploited combaining a proper orbit altitude ($600 - 800$ km) and inclination ($95 - 100$ deg), in this way the angle between the orbit plane and the line joining the Earth - Sun center remains constant. It is so clear that, with the opportune initial condition, the orbit can be chosen in order to allow the satellite to permanently face the Sun. Although it is a perfect condition for photovoltaic power generation, another important problem becomes evident. The solar power density right above the atmosphere at 1AU distance from the SUN is about 1.353 kW/m^2. In every real physical process, a 100% efficence is impossible and 50% conversions rates are very common. Photovoltaic energy transformation is even more critical in this regard, so that a large amount of this power will become heat. Even neglecting other thermal loads (like those caused by other satellite functions), a very critical amount of heat needs to be 'ejected' from the spacecraft. When dealing with 'normal' orbits and operational conditions, eclipse periods and/or satellites spin can be very useful to mitigate such problems. When dealing with SPS in Sun Synchronous Orbits though, these two positive factors vanish at the same time: the SPS would continously face the SUN in the very same config-

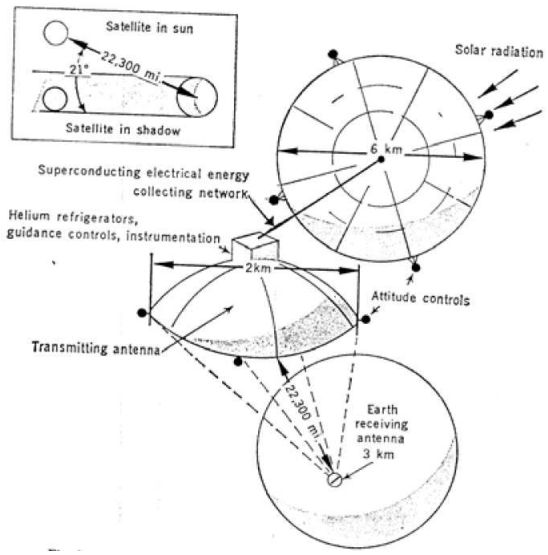

Figure 1.5: Glaser's First SPS Concept, Year 1968

uration (no spin). It si clear that particular effort has to be put in thermal management. Passive methods, such has multi layered insulation films or phase changing materials, would not be sufficient, so that active methods has to be implemented on board, typically cryogenic fluid coolers and fluid loops, coupled with louvers and heat pipes, are employed in this field. It should be clear that one 'face' of the satellite will permanently be heated, since it is continously directed towards the Sun, but, at the same time, the opposite 'face' will continuously be exposed to the deep space (except for particular cases where albedo and IR radiation from Earth or other celestial bodies have to be taken into account). So also the so called thermal gradient (the temperature difference and variation from one side of the spacecraft to the other) will be a critical stress factor for every satellite subsystem.

In these cases the most important task is to transport the heat from the hot face to the cold one, with a mean able to do the task quickly and in an efficient way. Due to the (hopefully) high amount of electrical energy available onboard, active thermal management system can be properly designed.

NASA-DOE SPS Reference Model

In their first important dedicated study, NASA and USA DOE developed the so called NASA - DOE SPS Reference Model (see fig. 1.6). This satellite is[25][26][18] a rectangular structure with a collector of 54.6 square kilometers

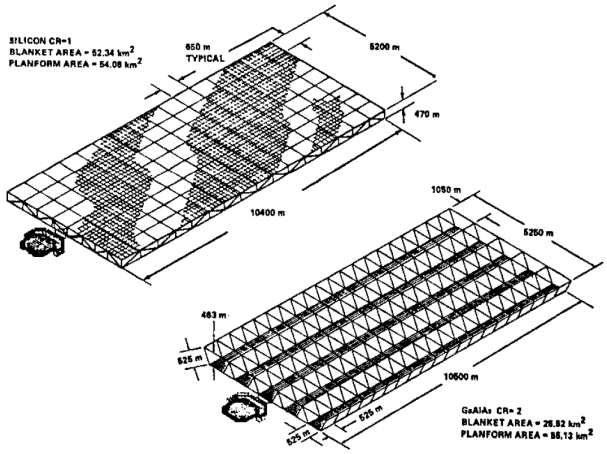

Figure 1.6: NASA-DOE SPS Reference Model, Year 1979

that has to receive solar energy from the Sun and to convert it into electric energy. The satellite has a microwave antenna to beam the energy to the Earth surface and it uses a mechanic steering system. A geostationary orbit is supposed for this concept with an active control system for both orbit and attitude station keeping. In fact it is really similar to Glaser's concept, except for the collector shape.

JAXA SPS 2000

The first Japanese concept appeared in the literature is the SPS 2000[24] (see fig. 1.7). This satellite flies in a medium Earth orbit (MEO), it is stabilized by means of gravity gradient torque, but the most important feature is that this satellite is the first one equipped with an electronic beam steering, this means that there is no more need of a critical element such as a mechanical joint able to make the antenna steer physically. This is a very relevant feature since it implies the elimination of a critical and heavy weight element. Obviously in this case there can not be a single rectenna on the surface receiving the electrical energy, but a set of different rectennas located along the ground track of the selected orbit.

NASA Solar Disc and NASA Sun Tower

Two new concepts appeared in 1997 proposed by NASA: Solar Disc[18] (fig. 1.8) and Sun Tower[18][6][19] (fig. 1.9). The former is a geostationary satellite, equipped with a high efficiency photo voltaic thin–film circular array, deployed in strips by means of the centrifugal force that arises when it is

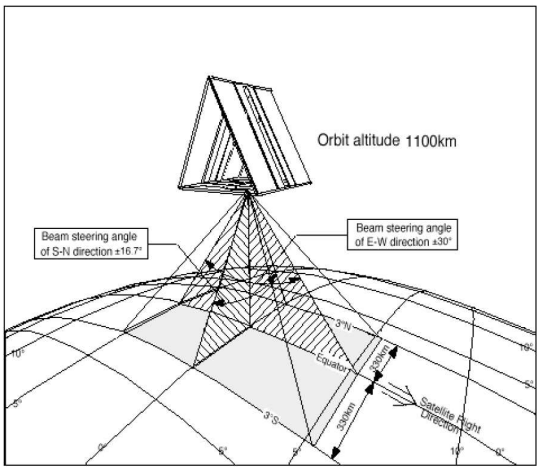

Figure 1.7: JAXA SPS 2000, Year 1991

rotating with respect to its center. The array is linked to the microwave antenna that rotates itself around the link axis in order to continuously face the Earth and to give the satellite gyroscopic stability, and it is equipped with an electronic beam steering system.

The Sun Tower is a structure composed by a 15 kilometers tether 'backbone' with the function of power management and distribution, it links a series of solar discs that have a diameter of 55 meters. These discs are thin film photo voltaic arrays able to rotate with respect to the arm which links them to the PMAD, in order to correctly face the Sun. At the lower end of the tether there is the microwave antenna which beams the electrical power down to the Earth, it is equipped with an electronic beam steering system. In this case the satellites are thought to compose a medium earth orbit constellation, so, also in this case, various rectennas on the surface near to the SPS ground track must be created. Both the satellites are gravity gradient stabilized.

Abacus Reflector

Another concept was proposed in year 2001, the Abacus Reflector[6]. This satellite has a rectangular solar collector of 10.24 square kilometers that convert the solar energy into electric one, which is then beamed to the Earth by means of a microwave antenna with a reflector used to mechanically steer the beam. It flies in a geostationary orbit.

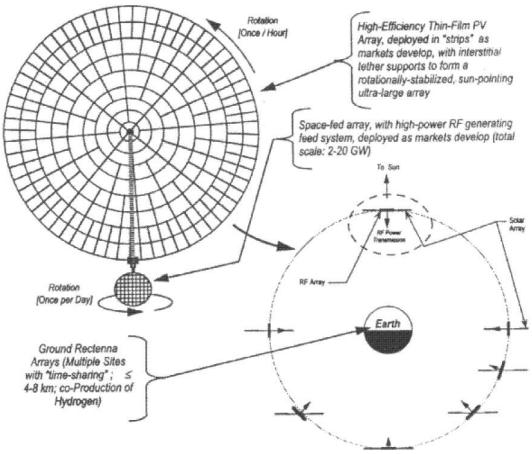

Figure 1.8: NASA Solar Disc, Year 1997

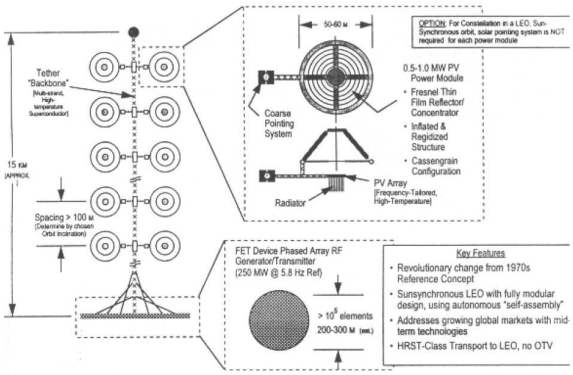

Figure 1.9: NASA Sun Tower, Year 1997

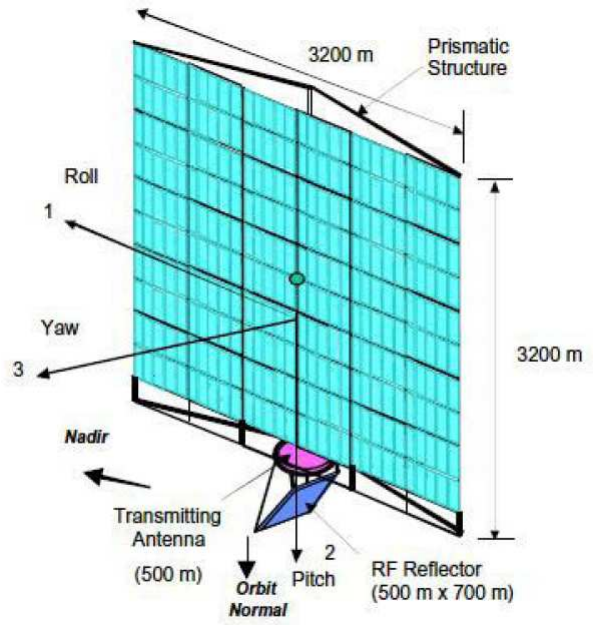

Figure 1.10: Abacus Reflector, Year 2001

European Sail Tower

The most important European concept is the Sail Tower[36][39]. This concept is similar to NASA Sun Tower, it has a 15 kilometers PMAD tether that constitute the backbone where different 'sails' are attached. These components transform solar energy into electric one, they can be oriented in order to continuously face the Sun. Also in this concept at the end of the PMAD there is the microwave antenna pointed towards the Earth. It flies in a geostationary orbit and it is gravity gradient stabilized.

JAXA Reference Model 2001

In year 2001 a new Japanese concept appeared, the JAXA Reference Model 2001[23]. This concept presents a collector area of 14 square kilometers composed by two symmetrical solar concentrators connected by means of a truss system, these elements focus the incoming solar radiation towards the central part of the structure that is equipped with a photo voltaic array which converts the solar energy into electrical one. On the other part of the array, which is conceived as a sandwich structure, it is mounted the microwave antenna that beams the energy to the surface and it is equipped with an electronic beam steering system. This satellite flies in a geostationary orbit.

Figure 1.11: European Sun Tower, Year 2001

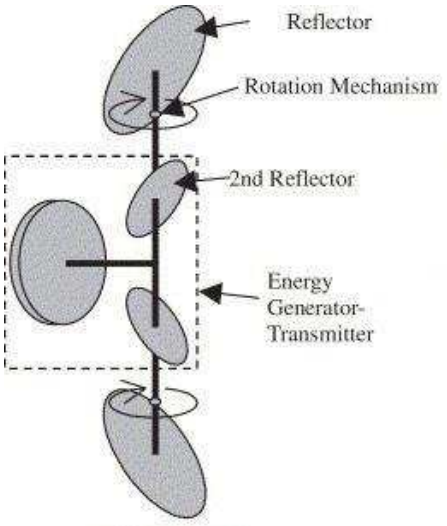

Figure 1.12: JAXA Reference Model, Year 2001

NASA Integrated Symmetrical Concentrator

The NASA Integrated Symmetrical Concentrator concept[6] is almost identical to the JAXA Reference Model 2001 except for the dimensions, in fact it has a collector area of about 1 square kilometer.

JAXA Reference Model 2003

In year 2003 a new Japanese concept appeared, the JAXA Reference Model 2003[8][23]. It may appear similar to the one proposed in 2001 but this

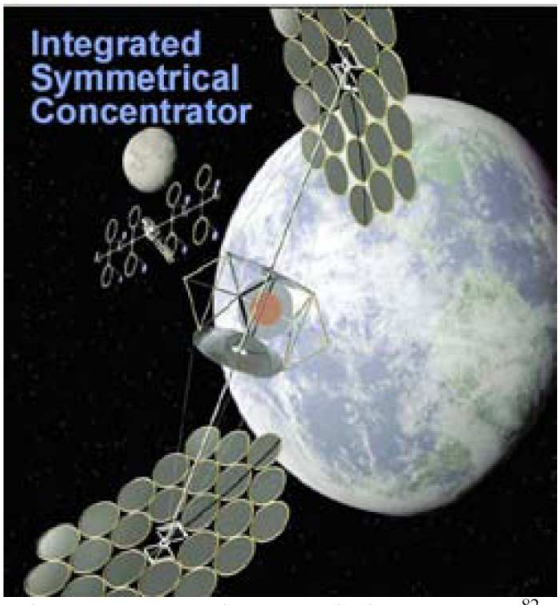

Figure 1.13: Integrated Symmetrical Concentrator, Year 2002

concept introduces an important new feature with respect to the others, it is the very first one that adopts the formation flying configuration. It is composed by three satellites, two solar collectors placed symmetrically with respect to the central one that is the sandwich panel which has on one side solar cells and on the other one the microwave antenna. The collectors total area is 14 square kilometers, and it is equipped with an electronic beam steering system. The central satellite flies in a common geostationary orbit while the other two satellites have to fly two non–Keplerian geostationary orbits.

Keplerian orbits are clear and simple to understand even after a very quick overview of the basic principles of orbital motion, i.e. the three Kepler's Laws. These simple principles, based on celestial bodies observation and data collection and then justified with the classical mechanics theory from Newton, state that every object in the two bodies problem (i.e. when only two celestial bodies are considered) moves drawing a conic section (ellipse/circle, parabola or hyerbola) with the central body in the focus of the given curve. So the motion is planar even if it takes place in the three dimensional space, the plane of motion can be identified for example by means of the position (the vector joining the two bodies centers) and velocity vectors. Since the motion will remain a planar one (if no other forces are applied to the system), also the attracting force must lay on the plane, in fact it is directed along the

position vector, it is quite clear that the central body will lie exacly on the plane of motion.

In order to understand non-Keplerian Orbits, it can be simpler to consider a particular case. For example in the case of this concept there will be three different objects orbiting around the central body (the Earth). The main object (the solar array) will fly a very common GEO Keplerian orbit, so that it will lie on the most classical plane of motion, the equatorial plane. The other two objects (the collectors) have to move togheter with the main one and to maintain a constant distance from it. This means that if the main object orbit is thought to be on an horizontal plane, the collectors would be over and below the solar array. In order to maintain this configuration, their orbits will need to take place in a plane parallel to the equatorial one, but shifted respectively up and down by a proper distance. The three planes cannot intersect, but this means that the central body (the Earth) cannot lay on the two collectors orbit planes, in fact they will fly two non-Keplerian Orbits. It is clear that also the gravitational force will not be contained in the orbital plane of the two collectors but it will have a component perpendicular to it. In order to recreate the two bodies dynamics, the planar motion condition has to be restored, it means that an out-of-plane thrust component has to be continously applied to the collectors to balance the gravity force component normal to the orbit planes to preserve their orbit.

Usually this force can be small (if compared with other forces), electrical propulsion, which combines high specific impulses (i.e. small fuel consumption) with small thrust, can be adopted exloiting the important amount of electrical power available on board.

JAXA Tethered SPS

In 2004 the Japanese Space Agency JAXA proposed another new SPS concept, the Tethered SPS[8][32]. This satellite is composed by a sandwich panel of 2.1 square kilometers with on one side solar cells and a microwave antenna on the other one, this panel is linked to a bus by means of four wires of 6 kilometers length, the bus hosts all other subsystems. It is equipped with an electronic beam steering system, it flies in a geostationary orbit and it is gravity gradient stabilized but the wires can be used as attitude controls too.

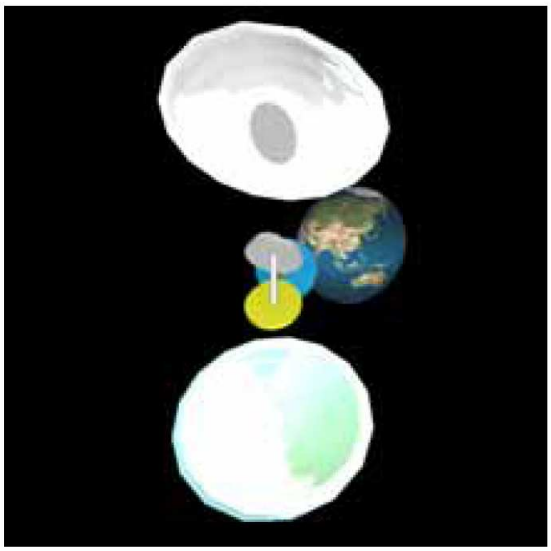

Figure 1.14: JAXA Reference Model, Year 2003

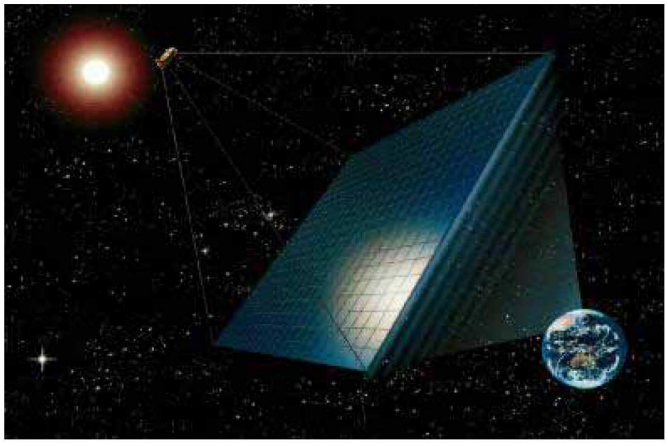

Figure 1.15: JAXA Tethered SPS, Year 2004

1.3 Work Objectives

This work will be focused on one of the previously described concepts, JAXA 2003 Reference Model, because of its modernity and appeal for the scientific community. As said before, this is the first SPS satellite with a formation flying configuration, composed by two symmetrical reflectors and a central array–panel flying in formation in a geostationary orbit. Given the dimensions of this satellites two main features arise:

- solar radiation acting on such large surfaces will cause a considerable orbit motion perturbation, acting continuously upon the spacecrafts;
- a model of flexible satellite should be adopted in order to evaluate attitude control related issues.

So that, this work main objectives will be oriented to spread the knowledge in these two fields, in order to give a contribution in the preliminary study of this concept:

- to develop a simple set of equations able to describe relative motion for formation flying satellites in case of orbital perturbations;
- to develop a new approach able to perform an optimal actuator placement for flexible structures.

In order to accomplish these objectives some particular instruments will be used, thus a brief resume of this particular knowledge will be given in few of the following chapters.

1.4 Thesis Structure

After this introduction, Chapter 2 addresses the issue of perturbed orbit propagation. A standard perturbation approach applied on classic orbital elements version of Gauss variational equations was developed during a previous work. Here it is recalled and it is integrated with a similar development performed on the time equation. So that a complete set of first–order approximated equations is available in order to analytically describe a perturbed orbit propagation. In Chapter 3 a new approach proposed by H. Schaub for relative motion description of formation flying satellites is recalled. It allows to obtain the propagation of the three Cartesian component in the LVLH reference frame starting from the knowledge of the initial difference in classical orbital elements between the satellites, when unperturbed flight is considered; in case of perturbations numerical integration must be performed. Its

formulation in terms of orbital elements and its use of the true anomaly ν as independent parameter, makes it attractive to be extended to perturbed orbital flight merging it with the standard perturbation approach discussed above. A simple analytical algorithm is developed, it is used to propagate the relative orbit of two formation flying satellite also in case of perturbation acting on them with an error lower than few percentage points ($< 2.5\%$). In Chapter 4 some basic concepts of Finite Element Methods are reported. In particular frames of beam elements are treated and a two–dimensional rectangular structure is modeled. The structure is described by means of mass, damping and stiffness matrices and a forces influence matrix. This model will be used in the actuator placement problem. In Chapter 5 a general overview of optimization methods is given, particular attention to stochastic algorithms is emphasized. In Chapter 6 some fundamentals instruments in Controllability of Dynamical Systems and Component Cost Analysis are presented. The discussion is than focused on second–order mechanical systems and actuator placement optimization. A case study is presented where the set of instruments presented in Chapters $4 - 6$ are applied. A two–dimensional flexible structure is first modeled by means of FEM like a frame of beams. Then, an actuator placement optimization problem is formalized by means of the *controllability* and *modal cost* concepts. Then, different optimization strategies are applied to obtain the most controllable system and compared one to each other in terms of solution accuracy and computational time. In particular, a classical approach presented in the literature is compared with three different kind of stochasic optimizators. Finally, in Chapter 7 a set of conclusions is presented and a roadmap on related and possible future works is drawn.

This page intentionally left blank

Chapter 2

Analytical Approximations for Perturbed Orbit Propagation

In this chapter the derivation of analytical relations for trajectory arcs with small perturbations by means of the perturbative approach is described briefly. The time equation will be investigated more accurately in order to obtain a significative improvement with respect to the previous work[28][1] where this approach was applied for the first time, since it will be really important in the formation flight. This theory could be applied both on the classical orbital elements and equinoctial orbital elements description of the spacecraft motion; since only the former set of elements is needed, it will be the only one recalled here, the other one being accurately described in[28].

The result provides a more accurate insight in the problem of the behavior description of a spacecraft under the action of small perturbations, particularly useful in the orbit propagation context.

2.1 Classical Orbital Parameter Formulation

Constant perturbing force $\vec{\boldsymbol{T}}$ is assumed, its orientation with respect to the radial direction $\hat{\boldsymbol{r}}$, the transverse one $\hat{\boldsymbol{\theta}}$ and normal to the orbit plane $\hat{\boldsymbol{w}}$ is defined by means of the following angles: α between the radial direction and the projection of the thrust vector on the $\hat{\boldsymbol{r}} - \hat{\boldsymbol{\theta}}$ plane, and β between the thrust vector and the $\hat{\boldsymbol{r}} - \hat{\boldsymbol{\theta}}$ plane (cf. fig 2.1). With this decomposition one can define the following quantities:

$$T_w = T \sin\beta; \quad T_r = T \cos\beta \cos\alpha; \quad T_\theta = T \cos\beta \sin\alpha$$

[1] Master Degree Thesis

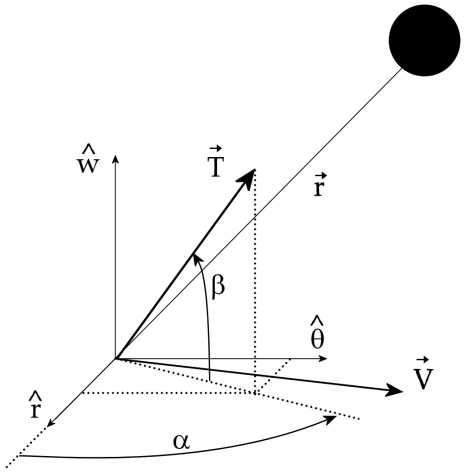

Figure 2.1: Force orientation

Force magnitude is made non–dimensional scaling it respect to the vehicle weight $\mu m/r^2$, that is a perturbation parameter

$$\varepsilon = \frac{T}{\mu m/r^2}$$

can be defined, which can be obviously seen as the ratio between the acceleration caused by the force and that caused by the gravitational attraction.

Classical orbital elements are one of the most used and clear way to represent orbital motion. It is a set of six parameters with a very intuitive meaning: a is the semi major axis, measure of the orbit dimension; e is the eccentricity, measure of the orbit shape; ω is the argument of perigee, it defines the angular position of the perigee (the direction of the closest point between the two bodies) in the orbital plane; i is the orbit inclination, it defines the orbit plane orientation in the three dimensional space; Ω is the ascending node right ascension, it defines the position of the orbital plane in the three dimensional space; and $\theta = \nu + \omega$ is the true latitude angle, sum of true anomaly (which measures the satellite angular travel on its orbit measured from the perigee) and argument of perigee, it defines the satellite position in the orbit. (See fig.2.2 for clarification)

The semi major axis a_0 of the initial orbit will be assumed as the reference length, while a mass parameter $\mu = 1$ is also assumed, such that the orbit period in non–dimensional terms is $\tau = 2\pi$ and the following derivation is independent of the particular celestial body considered.

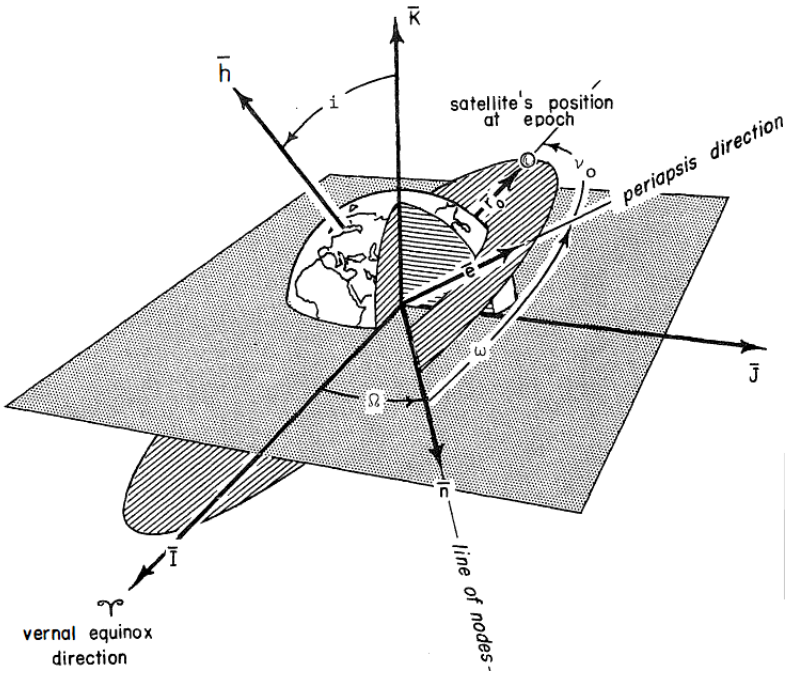

Figure 2.2: Classical Orbital Elements

Considering now Gauss's equations for variation of orbit parameters[2]

$$\begin{aligned}
\frac{d\Omega}{dt} &= \frac{r\sin(\nu+\omega)}{h\sin i}a_w \\
\frac{di}{dt} &= \frac{r\cos(\nu+\omega)}{h}a_w \\
\frac{d\omega}{dt} &= \frac{1}{he}\left[-p\cos\nu a_r + (p+r)\sin\nu a_\theta\right] - \frac{d\Omega}{dt}\cos i \\
\frac{da}{dt} &= \frac{2a^2}{h}\left(e\sin\nu a_r + \frac{p}{r}a_\theta\right) \\
\frac{de}{dt} &= \frac{1}{h}\left\{p\sin\nu a_r + \left[(p+r)\cos\nu + re\right]a_\theta\right\} \\
\frac{dM}{dt} &= n + \frac{b}{ahe}\left[(p\cos\nu - 2re)\,a_r - (p+r)\sin\nu a_\theta\right]
\end{aligned}$$

where the out-of-plane, radial and tangential acceleration components a_i, identified respectively via the subscripts $i = w, r, \theta$, can be replaced by the corresponding terms produced by the perturbing force that is $a_i = T_i/m$.

Replacing derivation with respect to time with derivation with respect to

the true anomaly by application of the chain rule

$$\frac{d}{dt} = \frac{d}{d\nu}\frac{d\nu}{dt} \Rightarrow \frac{d}{d\nu} = \frac{d}{dt}\frac{1}{\dot{\nu}}$$

one can rewrite the system of first order ordinary differential equations as follows:

$$\begin{aligned}
\frac{d\Omega}{d\nu} &= \frac{r^3 \sin(\nu+\omega)}{h^2 \sin i}\varepsilon \sin\beta \\
\frac{di}{d\nu} &= \frac{r^3 \cos(\nu+\omega)}{h^2}\varepsilon \sin\beta \\
\frac{d\omega}{d\nu} &= \frac{r^2}{h^2 e}\left[-p\cos\nu\varepsilon\cos\beta\cos\alpha + (p+r)\sin\nu\varepsilon\cos\beta\sin\alpha\right] - \frac{d\Omega}{d\nu}\cos i \\
\frac{da}{d\nu} &= \frac{2r^2a^2}{h^2}\left(e\sin\nu\varepsilon\cos\beta\cos\alpha + \frac{p}{r}\varepsilon\cos\beta\sin\alpha\right) \\
\frac{de}{d\nu} &= \frac{r^2}{h^2}\left\{p\sin\nu\varepsilon\cos\beta\cos\alpha + \left[(p+r)\cos\nu + re\right]\varepsilon\cos\beta\sin\alpha\right\} \\
\frac{dM}{d\nu} &= \frac{r^2}{a\sqrt{ap}} + \frac{\sqrt{ap}r^2}{ah^2e}\left[(p\cos\nu - 2re)\,\varepsilon\cos\beta\cos\alpha - (p+r)\sin\nu\varepsilon\cos\beta\sin\alpha\right]
\end{aligned}$$

where the quantities

$$\begin{aligned}
b &= \sqrt{pa} \\
h^2 &= p\mu \\
n &= h/ab \\
\dot{\nu} &= h/r^2
\end{aligned}$$

are used. In this case the equation for $\dot{\nu}$ contains only the zero–order term because the first–order one would not be taken into account when substituted in the equations above, giving raise only to second–order terms.

Then, introducing

$$\begin{aligned}
r &= \frac{p}{[1+e\cos\nu]} \\
p &= a\left(1-e^2\right) \\
h^2 &= p\mu
\end{aligned}$$

in the last system, it becomes

$$\begin{aligned}
\frac{d\Omega}{d\nu} &= \frac{a^2\left(1-e^2\right)^2\sin\left(\nu+\omega\right)}{\left[1+e\cos\left(\nu\right)\right]^3\sin i}\varepsilon\sin\beta \\
\frac{di}{d\nu} &= \frac{a^2\left(1-e^2\right)^2\cos\left(\nu+\omega\right)}{\left[1+e\cos\left(\nu\right)\right]^3}\varepsilon\sin\beta \\
\frac{d\omega}{d\nu} &= \frac{a\left(1-e^2\right)}{\left[1+e\cos\nu\right]^2 e}\left[-a\left(1-e^2\right)\cos\nu\varepsilon\cos\beta\cos\alpha+\right. \\
&+ \left. a\left(1-e^2\right)\left(1+\frac{1}{\left[1+e\cos\nu\right]}\right)\sin\nu\varepsilon\cos\beta\sin\alpha\right]-\frac{d\Omega}{d\nu}\cos i \\
\frac{da}{d\nu} &= \frac{2a^3\left(1-e^2\right)}{\left[1+e\cos\nu\right]^2}\left(e\sin\nu\varepsilon\cos\beta\cos\alpha+\left[1+e\cos\nu\right]\varepsilon\cos\beta\sin\alpha\right) \\
\frac{de}{d\nu} &= \frac{a\left(1-e^2\right)}{\left[1+e\cos\nu\right]^2}\left\{a\left(1-e^2\right)\sin\nu\varepsilon\cos\beta\cos\alpha+\right. \\
&+ \left[a\left(1-e^2\right)\left(1+\frac{1}{\left[1+e\cos\nu\right]}\right)\cos\nu+\right. \\
&+ \left.\left.\frac{ae(1-e^2)}{\left[1+e\cos\nu\right]}\right]\varepsilon\cos\beta\sin\alpha\right\} \\
\frac{dM}{d\nu} &= \frac{\sqrt{1-e^2}}{\left[1+e\cos\nu\right]^2}+\frac{\sqrt{(1-e^2)}a\left(1-e^2\right)}{e\left[1+e\cos\nu\right]^2}\left[a\left(1-e^2\right)\times\right. \\
&\times \left(\cos\nu-\frac{2e}{\left[1+e\cos\nu\right]}\right)\varepsilon\cos\beta\cos\alpha+ \\
&- \left. a\left(1-e^2\right)\left(1+\frac{1}{\left[1+e\cos\nu\right]}\right)\sin\nu\varepsilon\cos\beta\sin\alpha\right]
\end{aligned}$$

At this point the next step is to introduce the perturbative expansions for all the orbital parameters and to substitute these relations into the differential equation system. The expansions are truncated to first–order terms, so they are written as

$$\begin{aligned}
a &= a_0+\varepsilon a_1 \\
e &= e_0+\varepsilon e_1 \\
i &= i_0+\varepsilon i_1 \\
\omega &= \omega_0+\varepsilon\omega_1 \\
\Omega &= \Omega_0+\varepsilon\Omega_1 \\
M &= M_0+\varepsilon M_1
\end{aligned}$$

Introducing them into the previous differential equation system (the symbol ' denote the derivation with respect to ν) and expressing only those factors that give rise to first–order terms one obtains

$$\begin{aligned}
\Omega_0' + \varepsilon\Omega_1' &= \frac{a_0^2\left(1-e_0^2\right)^2 \sin\left(\nu+\omega_0\right)}{\left[1+e_0\cos\left(\nu\right)\right]^3 \sin i_0}\varepsilon\sin\beta \\
i_0' + \varepsilon i_1' &= \frac{a_0^2\left(1-e_0^2\right)^2 \cos\left(\nu+\omega_0\right)}{\left[1+e_0\cos\left(\nu\right)\right]^3}\varepsilon\sin\beta \\
\omega_0' + \varepsilon\omega_1' &= \frac{a_0\left(1-e_0^2\right)}{\left[1+e_0\cos\nu\right]^2 e_0}\left[-a_0\left(1-e_0^2\right)\cos\nu\varepsilon\cos\beta\cos\alpha+\right. \\
&+ \left. a_0\left(1-e_0^2\right)\left(1+\frac{1}{\left[1+e_0\cos\nu\right]}\right)\sin\nu\varepsilon\cos\beta\sin\alpha\right]+ \\
&- \Omega_0'\cos i_0 - \varepsilon\Omega_1'\cos i_0 \\
a_0' + \varepsilon a_1' &= \frac{2a_0^3\left(1-e_0^2\right)}{\left[1+e_0\cos\nu\right]^2}\left(e_0\sin\nu\varepsilon\cos\beta\cos\alpha+\left[1+e_0\cos\nu\right]\varepsilon\cos\beta\sin\alpha\right) \\
e_0' + \varepsilon e_1' &= \frac{a_0\left(1-e_0^2\right)}{\left[1+e_0\cos\nu\right]^2}\left\{a_0\left(1-e_0^2\right)\sin\nu\varepsilon\cos\beta\cos\alpha+\right. \\
&+ \left.\left[a_0\left(1-e_0^2\right)\left(1+\frac{1}{\left[1+e_0\cos\nu\right]}\right)\cos\nu+\frac{a_0e_0(1-e_0^2)}{\left[1+e_0\cos\nu\right]}\right]\varepsilon\cos\beta\sin\alpha\right\} \\
M_0' + \varepsilon M_1' &= \frac{\sqrt{1-e^2}}{\left[1+e\cos\nu\right]^2}+\frac{a_0\left(1-e_0^2\right)^{3/2}}{e_0\left[1+e_0\cos\nu\right]^2}\left[a_0\left(1-e_0^2\right)\left(\cos\nu-\frac{2e_0}{\left[1+e_0\cos\nu\right]}\right)\times\right. \\
&\times \left.\varepsilon\cos\beta\cos\alpha-a_0\left(1-e_0^2\right)\left(1+\frac{1}{\left[1+e_0\cos\nu\right]}\right)\sin\nu\varepsilon\cos\beta\sin\alpha\right]
\end{aligned}$$

At this point it is introduced the improvement with respect to the previous formulation. One can note that once ν is known the information given by the last quantity M is redundant, i.e. not strictly necessary to define vehicle position, so that it will be neglected in what follows. This fact apparently allows one to ignore one equation with no loss of information, but this is not the case: another equation is needed to close the system in time, which is derived from the one used to perform the change in derivation variable by means of the chain rule, that is:

$$\frac{1}{\dot{\nu}} = \frac{r^2}{h}+\frac{\sqrt{h}e}{p}\frac{1}{\varepsilon\left(\cos\nu\cos\beta\cos\alpha-\dfrac{2+e\cos\nu}{1+e\cos\nu}\sin\nu\cos\beta\sin\alpha\right)}$$

and this time the first–order term is fundamental in order to take into account all due contributions.

With this strategy, one change the focus from time as independent variable to ν, so it is for this reason that the equation for M is apparently not needed anymore, but, in doing this, time becomes a dependent variable, and an equation is needed to evaluate it. Using the previous relation and the previous defined quantities (expressed as functions of ν) one can write

$$\frac{dt}{d\nu} = \frac{r^2}{h} + \frac{\sqrt{h}e}{p} \frac{1}{\varepsilon \left(\cos\nu\cos\beta\cos\alpha - \dfrac{2+e\cos\nu}{1+e\cos\nu}\sin\nu\cos\beta\sin\alpha \right)}$$

which is an equation similar to the others, where one can introduce an approximate perturbative expansion for the time:

$$t = t_0 + \varepsilon t_1$$

Upon substitution, one can obtain the perturbed variation of time in the exact same way of the other parameters.

Solving for the terms of zero order one obtains

$$\begin{aligned}
a_0 &= \bar{a}_0 \\
e_0 &= \bar{e}_0 \\
i_0 &= \bar{i}_0 \\
\omega_0 &= \bar{\omega}_0 \\
\Omega_0 &= \bar{\Omega}_0 \\
t_0 &= \frac{\bar{p}_0^2}{\bar{h}_0} \int_{\nu_0}^{\nu} \frac{1}{\left[1+\bar{e}_0\cos\nu\right]^2}
\end{aligned}$$

where the values with the over bar are referred to quantities assigned at the initial time $\bar{t}_0$ (from now on this notation will be omitted and all values with subscript 0 will be quantities evaluated at initial time). For the first–order

terms one gets

$$
\begin{aligned}
\Omega_1 &= \frac{a_0^2\left(1-e_0^2\right)^2\sin\beta}{\sin i_0}\left[\cos\omega_0\int_{\nu_0}^{\nu}\frac{\sin\nu}{\left[1+e_0\cos\nu\right]^3}+\sin\omega_0\int_{\nu_0}^{\nu}\frac{\cos\nu}{\left[1+e_0\cos\nu\right]^3}\right]\\
i_1 &= a_0^2\left(1-e_0^2\right)^2\sin\beta\left[\cos\omega_0\int_{\nu_0}^{\nu}\frac{\cos\nu}{\left[1+e_0\cos\nu\right]^3}-\sin\omega_0\int_{\nu_0}^{\nu}\frac{\sin\nu}{\left[1+e_0\cos\nu\right]^3}\right]\\
\omega_1 &= -\frac{a_0^2\left(1-e_0^2\right)^2\cos\beta\cos\alpha}{e_0}\int_{\nu_0}^{\nu}\frac{\cos\nu}{\left[1+e_0\cos\nu\right]^2}+\\
&+ \frac{a_0^2\left(1-e_0^2\right)^2\cos\beta\sin\alpha}{e_0}\left[\int_{\nu_0}^{\nu}\frac{\sin\nu}{\left[1+e_0\cos\nu\right]^2}+\int_{\nu_0}^{\nu}\frac{\sin\nu}{\left[1+e_0\cos\nu\right]^3}\right]\\
&- \left(\Omega_1-\Omega_{1_0}\right)\cos i_0\\
a_1 &= 2a_0^3\left(1-e_0^2\right)e_0\cos\beta\cos\alpha\int_{\nu_0}^{\nu}\frac{\sin\nu}{\left[1+e_0\cos\nu\right]^2}+\\
&+ 2a_0^3\left(1-e_0^2\right)\cos\beta\sin\alpha\int_{\nu_0}^{\nu}\frac{1}{\left[1+e_0\cos\nu\right]}\\
e_1 &= a_0^2\left(1-e_0^2\right)^2\cos\beta\cos\alpha\int_{\nu_0}^{\nu}\frac{\sin\nu}{\left[1+e_0\cos\nu\right]^2}+\\
&+ a_0^2\left(1-e_0^2\right)^2\cos\beta\sin\alpha\left[\int_{\nu_0}^{\nu}\frac{\cos\nu}{\left[1+e_0\cos\nu\right]^2}+\int_{\nu_0}^{\nu}\frac{\cos\nu}{\left[1+e_0\cos\nu\right]^3}\right]+\\
&+ a_0^2\left(1-e_0^2\right)^2e_0\cos\beta\sin\alpha\int_{\nu_0}^{\nu}\frac{1}{\left[1+e_0\cos\nu\right]^3}\\
t_1 &= \frac{p^5}{h^3}\left(\cos\alpha\int_{\nu_0}^{\nu}\frac{\cos\nu}{\left[1+e_0\cos\nu\right]^4}-\sin\alpha\left(\int_{\nu_0}^{\nu}\frac{\sin\nu}{\left[1+e_0\cos\nu\right]^4}+\right.\right.\\
&+ \left.\left.\int_{\nu_0}^{\nu}\frac{\sin\nu}{\left[1+e_0\cos\nu\right]^5}\right)\right)+f\left(a_0,e_0,i_0,\omega_0,\Omega_0,\nu,\alpha,\beta\right)
\end{aligned}
$$

where f in the expression of t_1 is a very complex term:

$$
\begin{aligned}
f &= \frac{p_0}{2h_0}\left(C_{Is2c}I_{s2c}+C_{11c}I_{11c}+C_{13c}I_{13c}+C_{c2c}I_{c2c}+C_{c3c}I_{c3c}+C_{Is2u}I_{s2u}+\right.\\
&+ \left.C_{11u}I_{11u}+C_{13u}I_{13u}+C_{c2u}I_{c2u}+C_{c3u}I_{c3u}\right)
\end{aligned}
$$

with

$$
\begin{aligned}
C_{Is2c} &= \cos\beta\cos\alpha\,(2a_0k_e\,(e_0^2+2)+3e_0^2k_a\,(e_0^2-1)) \\
C_{11c} &= \cos\beta\sin\alpha\;3e_0k_a\,(e_0^2-1) \\
C_{13c} &= \cos\beta\sin\alpha\;e_0 2a_0k_e\,(e_0^2+2) \\
C_{c2c} &= \cos\beta\sin\alpha\;2a_0k_e\,(e_0^2+2) \\
C_{c3c} &= \cos\beta\sin\alpha\;2a_0k_e\,(e_0^2+2) \\
C_{Is2u} &= \cos\beta\cos\alpha\;3e_0\,(2a_0k_e+k_a\,(e_0^2-1)) \\
C_{11u} &= \cos\beta\sin\alpha\;3k_a\,(e_0^2-1) \\
C_{13u} &= \cos\beta\sin\alpha\;6a_0e_0^2k_e \\
C_{c2u} &= \cos\beta\sin\alpha\;6a_0e_0k_e \\
C_{c3u} &= \cos\beta\sin\alpha\;6a_0e_0k_e
\end{aligned}
$$

where

$$
\begin{aligned}
k_a &= 2a_0^2p_0^2/h_0^2 \\
k_e &= p_0^2/h_0^2
\end{aligned}
$$

and

$$
\begin{aligned}
I_{s2c} &= \int_{\nu_0}^{\nu} \left(\frac{\cos\nu}{\left[1+e_0\cos\nu\right]^3} \int \frac{\sin\nu}{\left[1+e_0\cos\nu\right]^2} d\nu \right) d\nu - I_{s20} \int_{\nu_0}^{\nu} \frac{\cos\nu}{\left[1+e_0\cos\nu\right]^3} d\nu \\
I_{11c} &= \int_{\nu_0}^{\nu} \left(\frac{\cos\nu}{\left[1+e_0\cos\nu\right]^3} \int \frac{1}{\left[1+e_0\cos\nu\right]} d\nu \right) d\nu - I_{110} \int_{\nu_0}^{\nu} \frac{\cos\nu}{\left[1+e_0\cos\nu\right]^3} d\nu \\
I_{13c} &= \int_{\nu_0}^{\nu} \left(\frac{\cos\nu}{\left[1+e_0\cos\nu\right]^3} \int \frac{1}{\left[1+e_0\cos\nu\right]^3} d\nu \right) d\nu - I_{130} \int_{\nu_0}^{\nu} \frac{\cos\nu}{\left[1+e_0\cos\nu\right]^3} d\nu \\
I_{c2c} &= \int_{\nu_0}^{\nu} \left(\frac{\cos\nu}{\left[1+e_0\cos\nu\right]^3} \int \frac{\cos\nu}{\left[1+e_0\cos\nu\right]^2} d\nu \right) d\nu - I_{c20} \int_{\nu_0}^{\nu} \frac{\cos\nu}{\left[1+e_0\cos\nu\right]^3} d\nu \\
I_{c3c} &= \int_{\nu_0}^{\nu} \left(\frac{\cos\nu}{\left[1+e_0\cos\nu\right]^3} \int \frac{\cos\nu}{\left[1+e_0\cos\nu\right]^3} d\nu \right) d\nu - I_{c30} \int_{\nu_0}^{\nu} \frac{\cos\nu}{\left[1+e_0\cos\nu\right]^3} d\nu \\
I_{s2u} &= \int_{\nu_0}^{\nu} \left(\frac{1}{\left[1+e_0\cos\nu\right]^3} \int \frac{\sin\nu}{\left[1+e_0\cos\nu\right]^2} d\nu \right) d\nu - I_{s20} \int_{\nu_0}^{\nu} \frac{1}{\left[1+e_0\cos\nu\right]^3} d\nu \\
I_{11u} &= \int_{\nu_0}^{\nu} \left(\frac{1}{\left[1+e_0\cos\nu\right]^3} \int \frac{1}{\left[1+e_0\cos\nu\right]} d\nu \right) d\nu - I_{110} \int_{\nu_0}^{\nu} \frac{1}{\left[1+e_0\cos\nu\right]^3} d\nu \\
I_{13u} &= \int_{\nu_0}^{\nu} \left(\frac{1}{\left[1+e_0\cos\nu\right]^3} \int \frac{1}{\left[1+e_0\cos\nu\right]^3} d\nu \right) d\nu - I_{130} \int_{\nu_0}^{\nu} \frac{1}{\left[1+e_0\cos\nu\right]^3} d\nu \\
I_{c2u} &= \int_{\nu_0}^{\nu} \left(\frac{1}{\left[1+e_0\cos\nu\right]^3} \int \frac{\cos\nu}{\left[1+e_0\cos\nu\right]^2} d\nu \right) d\nu - I_{c20} \int_{\nu_0}^{\nu} \frac{1}{\left[1+e_0\cos\nu\right]^3} d\nu \\
I_{c3u} &= \int_{\nu_0}^{\nu} \left(\frac{1}{\left[1+e_0\cos\nu\right]^3} \int \frac{\cos\nu}{\left[1+e_0\cos\nu\right]^3} d\nu \right) d\nu - I_{c30} \int_{\nu_0}^{\nu} \frac{1}{\left[1+e_0\cos\nu\right]^3} d\nu
\end{aligned}
\tag{2.1}
$$

and

$$
\begin{aligned}
I_{s20} &= \int \frac{\sin\nu}{\left[1+e_0\cos\nu\right]^2} d\nu \Bigg|_{\nu_0} \\
I_{110} &= \int \frac{1}{\left[1+e_0\cos\nu\right]} d\nu \Bigg|_{\nu_0} \\
I_{130} &= \int \frac{1}{\left[1+e_0\cos\nu\right]^3} d\nu \Bigg|_{\nu_0} \\
I_{c20} &= \int \frac{\cos\nu}{\left[1+e_0\cos\nu\right]^2} d\nu \Bigg|_{\nu_0} \\
I_{c30} &= \int \frac{\cos\nu}{\left[1+e_0\cos\nu\right]^3} d\nu \Bigg|_{\nu_0}
\end{aligned}
$$

Noticing that

$$\begin{aligned}\frac{\sin(\nu+\omega_0)}{[1+e_0\cos\nu]^3} &= \frac{\sin\nu\cos\omega_0+\cos\nu\sin\omega_0}{[1+e_0\cos\nu]^3}\\ \frac{\cos(\nu+\omega_0)}{[1+e_0\cos\nu]^3} &= \frac{\cos\nu\sin\omega_0-\sin\nu\cos\omega_0}{[1+e_0\cos\nu]^3}\end{aligned}$$

the complete solution of the problem requires to solve the integrals present in the equations of the first–order terms. All of them have an analytical solution except for the first integrals on each row of equations 2.1 that are part of the term f in the equation for t_1. It has been verified, as it will be shown in the next section, that this term f is quite important in order to improve the precision of the time evaluation as a function of ν, but at the same time it needs numerical evaluation of those quantities that results in additional computational time. Thus the user has to choose between a more accurate time evaluation with a higher computational time (even if it remains about the 5% of the computational time required by the numerical integration) or a less accurate solution with a computational time equal to the 0.02% of the numerical integration time.

$$\begin{aligned}\int\frac{\sin\nu}{[1+e_0\cos\nu]^2}d\nu &= \frac{1}{e_0(1+e_0\cos\nu)}\\ \int\frac{\sin\nu}{[1+e_0\cos\nu]^3}d\nu &= \frac{1}{2e_0(1+e_0\cos\nu)^2}\\ \int\frac{1}{[1+e_0\cos\nu]}d\nu &= \frac{\nu}{\sqrt{1-e_0^2}}-\frac{2\arctan\left(\frac{2e_0\sin\nu}{2e_0\cos\nu+\left(\sqrt{1-e_0}+\sqrt{1+e_0}\right)^2}\right)}{\sqrt{1-e_0^2}}\\ \int\frac{1}{[1+e_0\cos\nu]^2}d\nu &= -\frac{2\arctan\left(\frac{2e_0\sin\nu}{2e_0\cos\nu+\left(\sqrt{1-e_0}+\sqrt{1+e_0}\right)^2}\right)}{(1-e_0^2)^{3/2}}+\\ &+ \frac{e_0\sin\nu}{(e_0^2-1)(1+e_0\cos\nu)}+\frac{\nu}{(1-e_0^2)^{3/2}}\end{aligned}$$

$$
\begin{aligned}
\int \frac{1}{\left[1+e_0\cos\nu\right]^3}d\nu &= \left(\frac{1}{\left(1-e_0^2\right)^{3/2}}-\frac{3}{\left(1-e_0^2\right)^{5/2}}\right)\times \\
&\times \arctan\left(\frac{2e_0\sin\nu}{2e_0\cos\nu+\left(\sqrt{1-e_0}+\sqrt{e_0+1}\right)^2}\right)+ \\
&- \frac{e_0\sin\nu\left(3e_0\cos\nu-e_0^2+4\right)}{2\left(e_0^2-1\right)^2\left(1+e_0\cos\nu\right)^2}-\frac{\nu}{2\left(1-e_0^2\right)^{3/2}}+\frac{3\nu}{2\left(1-e_0^2\right)^{5/2}} \\
\int \frac{\cos\nu}{\left[1+e_0\cos\nu\right]^2}d\nu &= \left(\frac{2}{e_0\left(1-e_0^2\right)^{3/2}}-\frac{2}{e_0\sqrt{1-e_0^2}}\right)\times \\
&\times \arctan\left(\frac{2e_0\sin\nu}{2e_0\cos\nu+\left(\sqrt{1-e_0}+\sqrt{e_0+1}\right)^2}\right)+ \\
&+ \frac{\sin\nu}{\left(1-e_0^2\right)\left(1+e_0\cos\nu\right)}+\frac{\nu}{e_0\sqrt{1-e_0^2}}-\frac{\nu}{e_0\left(1-e_0^2\right)^{3/2}} \\
\int \frac{\cos\nu}{\left[1+e_0\cos\nu\right]^3}d\nu &= \left(\frac{e_0^2+2}{e_0\left(1-e_0^2\right)^{5/2}}-\frac{2}{e_0\left(1-e_0^2\right)^{3/2}}\right)\times \\
&\times \arctan\left(\frac{2e_0\sin\nu}{2e_0\cos\nu+\left(\sqrt{1-e_0}+\sqrt{e_0+1}\right)^2}\right)+ \\
&+ \frac{\sin\nu\left(e_0\left(2e_0^2+1\right)\cos\nu+e_0^2+2\right)}{2\left(e_0^2-1\right)^2\left(1+e_0\cos\nu\right)^2}+ \\
&+ \frac{3\nu}{2e_0\left(1-e_0^2\right)^{3/2}}-\frac{3\nu}{2e_0\left(1-e_0^2\right)^{5/2}} \\
\int \frac{\cos\nu}{\left[1+e_0\cos\nu\right]^4}d\nu &= \left(\frac{3e_0^2+2}{e_0\left(1-e_0\right)^{7/2}\left(e_0+1\right)^{7/2}}-\frac{e_0^2+2}{e_0\left(1-e_0\right)^{5/2}\left(e_0+1\right)^{5/2}}\right)\times \\
&\times \arctan\left(\frac{2e_0\sin\nu}{2e_0\cos\nu+\left(\sqrt{1-e_0}+\sqrt{e_0+1}\right)^2}\right)+ \\
&+ \sin\nu\frac{\left(52e_0^4+8e_0^2+7\right)\cos^2\nu-12e_0\left(e_0^4-9e_0^2-2\right)\cos\nu}{24\left(e_0+1\right)^3\left(1-e_0\right)^3\left(e_0\cos\nu+1\right)^3}+ \\
&- \frac{\nu}{2e_0\left(1-e_0\right)^{3/2}\left(e_0+1\right)^{3/2}}+\frac{3\nu}{e_0\left(1-e_0\right)^{5/2}\left(e_0+1\right)^{5/2}}+ \\
&- \frac{5\nu}{2e_0\left(1-e_0\right)^{7/2}\left(e_0+1\right)^{7/2}}+\frac{7\sin^2\nu-4e_0^4+40e_0^2+17}{24\left(e_0+1\right)^3\left(1-e_0\right)^3\left(e_0\cos\nu+1\right)^3} \\
\int \frac{\sin\nu}{\left[1+e_0\cos\nu\right]^4}d\nu &= \frac{1}{3e_0\left(e_0\cos\nu+1\right)^3} \\
\int \frac{\sin\nu}{\left[1+e_0\cos\nu\right]^5}d\nu &= \frac{1}{4e_0\left(e_0\cos\nu+1\right)^4}
\end{aligned}
$$

In order to obtain a formulation valid for thrust components projected

along the velocity-normal frame, one can transform Gauss's equations by means of a rotation matrix that transforms the vectors expressed with respect to $\hat{\boldsymbol{r}} - \hat{\boldsymbol{\theta}}$ into frame components expressed with respect to the direction of the velocity and in–plane normal direction unit vectors:

$$\begin{bmatrix} a_{dr} \\ \\ a_{d\theta} \end{bmatrix} = \frac{h}{pv} \begin{bmatrix} e\sin\nu & -(1+e\cos\nu) \\ \\ 1+e\cos\nu & e\sin\nu \end{bmatrix} \begin{bmatrix} a_{dt} \\ \\ a_{dn} \end{bmatrix}$$

thus obtaining the equations reported in [2]. Expressing v as a function of the orbit parameters one can apply the same perturbative technique, but in this case no analytical result would be obtained.

2.2 Results

In this section some results are presented. First of all a general case is considered (see fig 2.3), the perturbing force is applied in a general direction ($\alpha = 90\ deg$ and $\beta = 20\ deg$) and with a perturbation parameter of $\varepsilon = 10^{-4}$. In figure 2.3 there is the comparison between the numerical evaluations of orbital parameters variation (dotted line), obtained applying a common integration scheme for ordinary differential equation (it is MATLAB©ode45) on Gauss' equations, and the approximated relations developed by perturbation theory (solid line).

The simulation run covered about five orbits, it is quite clear how the two expressions are really near and how well the approximated relations describe also the sub–orbital motion, not only the terms secular variation. A more detailed discussion about the error of this approach (with the analysis of errors as a function of ε, in case of different force orientation, with both equinoctial and classical parameters, etc.) can be found in [28].

The second aspect that is analyzed hereafter regards the time equation. As said before a rigorous first–order formulation has been carried out, the drawback is the need of numerical integration for some integrals that arise in one first–order term in the expression of approximated time of flight. Even with this additional numerical calculation the approximated first–order relation is 20 times faster than the classical numerical integration. Anyway without it the approximated relation would be 5000 times faster than the classical numerical integration (due to the closed solution of all the integrals). So that it is necessary to verify how important is the non–analytical part of the time approximated expression.

In figures 2.4, 2.5 and 2.6 it can be seen the comparison between three quantities: the dotted line is the time of flight as a function of true anomaly ν

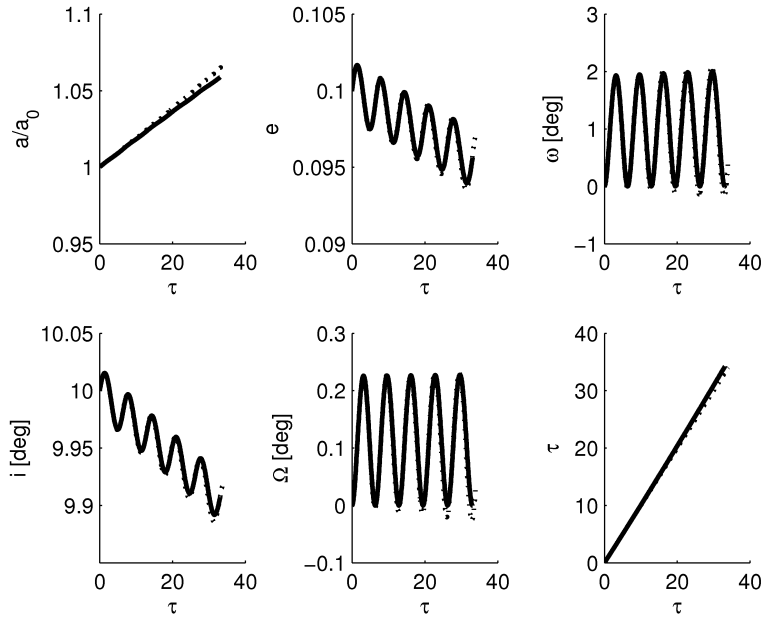

Figure 2.3: Comparison between approximated relations (solid line) and numerical integration (dotted line), $\alpha = 90\ deg$ and $\beta = 20\ deg$

evaluated numerically (i.e. the accurate reference value); the solid line is the time of flight evaluated with the complete rigorous first–order approximated expression and the dashed line represents the time of flight evaluated using the first–order approximated expression without the contribution of the non–analytical term (called 'simplified' from now on). It is quite clear how, even if the error remains small, the simplified relation is noticeably improved when the numerical term is added. For this reason it will be on the user call the use of one approximated expression or the other, depending on both required accuracy and need to save computational time.

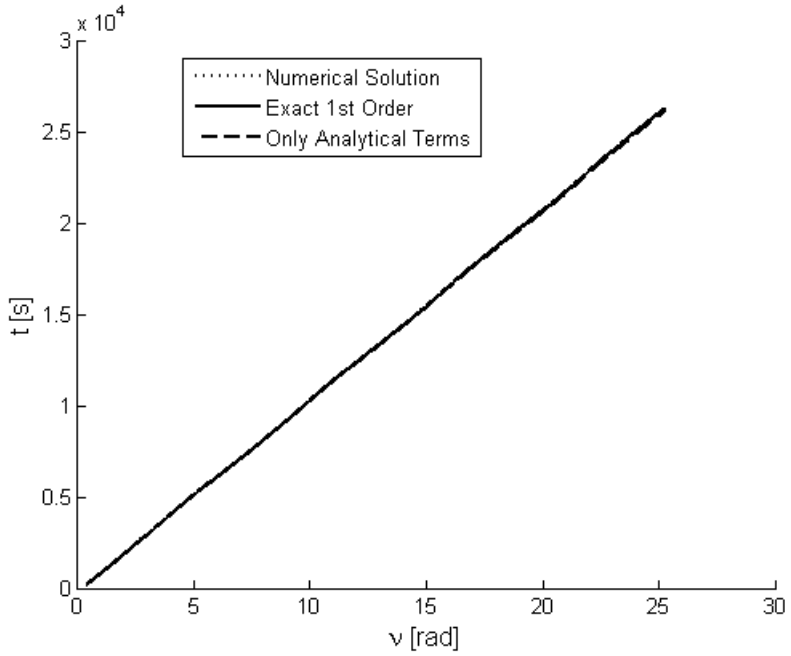

Figure 2.4: Time function of ν

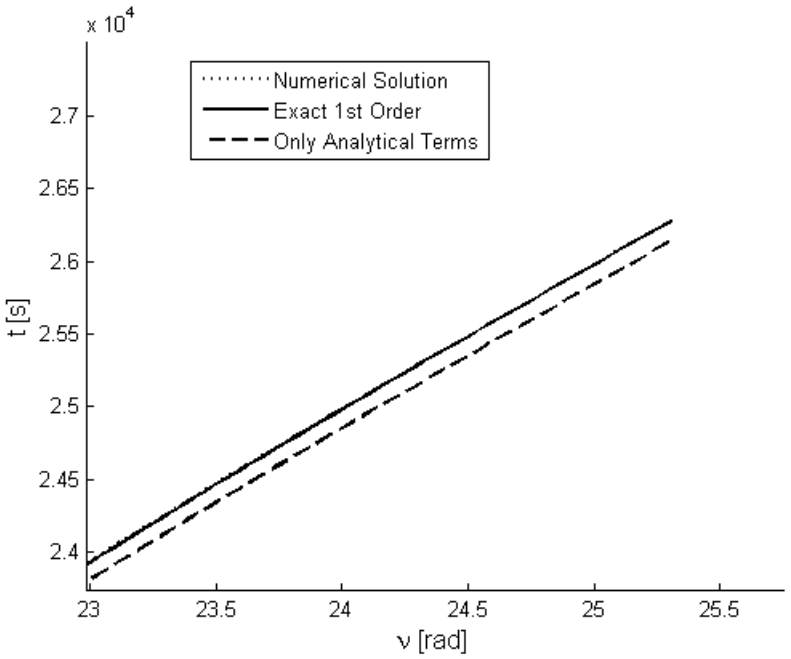

Figure 2.5: Time function of ν

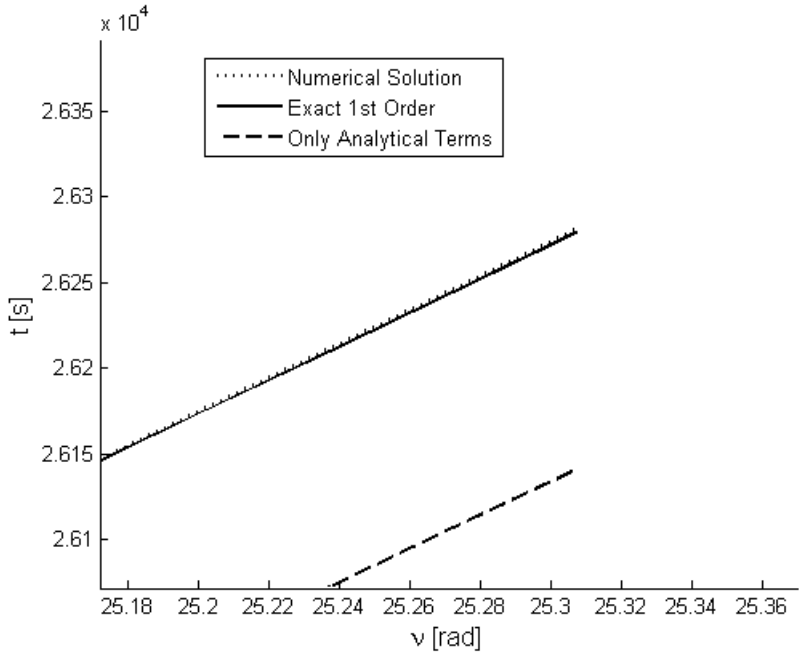

Figure 2.6: Time function of ν

This page intentionally left blank

Chapter 3

Formation Flying SPS

3.1 Schaub's Formulation

Hereafter Schaub's formulation is reported as described in [33][34][35]. This set of equations describes the relative orbit of a deputy satellite around a chief one by means of classical orbital elements difference between two spacecrafts.

The LVLH reference frame will be considered in order to derive the equations. The x-axis is the radial direction from the center of the Earth to the chief satellite, the z-axis is aligned with the chief momentum vector and the y-axis completes the frame with the right hand rule. The orbit element vector is given by

$$\boldsymbol{e} = (a, \theta, i, q_1, q_1, \Omega) \tag{3.1}$$

with

$$q_1 = e\cos\omega \tag{3.2}$$

$$q_2 = e\sin\omega \tag{3.3}$$

Because of the small difference between the satellites orbital elements, it is possible to write

$$\boldsymbol{e}_d = \boldsymbol{e}_c + \delta\boldsymbol{e} \tag{3.4}$$

where the subscript d denotes deputy satellite quantities while c chief ones. Superscripts $\mathcal{C}$ and $\mathcal{D}$ denotes quantities described respectively in the chief and deputy LVLH reference frames, and $\mathcal{N}$ will be referred to the inertial frame. Then $T^{\mathcal{CN}} = T^{\mathcal{CN}}(\Omega_c, i_c, \theta_c)$ is the matrix which transforms quantities from the inertial reference frame to the LVLH one. In order to obtain the relative motion relations, deputy satellite position is written in both LVLH reference frames

$${}^{\mathcal{C}}\boldsymbol{r}_d = {}^{\mathcal{C}}(R_c + x, y, z)^T \tag{3.5}$$

$${}^{\mathcal{D}}\boldsymbol{r}_d = {}^{\mathcal{D}}(R_d, 0, 0)^T \tag{3.6}$$

where R is the inertial radius. The relation between the two previous quantities is given by the following relation

$$^{\mathcal{C}}\boldsymbol{r}_d = T^{\mathcal{CN}} T^{\mathcal{ND}}\ ^{\mathcal{D}}\boldsymbol{r}_d \tag{3.7}$$

Dropping the c subscript, from now on all quantities without a subscript will be referred to the chief satellite. Considering the first variation of $T^{\mathcal{ND}}$ and R_d leads to the first order approximations

$$T^{\mathcal{ND}} \approx T^{\mathcal{NC}} + \delta T^{\mathcal{NC}} \tag{3.8}$$

$$R_d \approx R + \delta R \tag{3.9}$$

Equation 3.7 can be written as

$$^{\mathcal{C}}\boldsymbol{r}_d = \left(I_{3\ X\ 3} + T^{\mathcal{CN}} \delta T^{\mathcal{NC}}\right) (R + \delta R, 0, 0)^T \tag{3.10}$$

and neglecting second order terms deputy position can be expressed as

$$^{\mathcal{C}}\boldsymbol{r}_d = \begin{pmatrix} R + \delta R \\ 0 \\ 0 \end{pmatrix} + R T^{\mathcal{CN}} \begin{pmatrix} \delta T_{11}^{\mathcal{NC}} \\ \delta T_{21}^{\mathcal{NC}} \\ \delta T_{31}^{\mathcal{NC}} \end{pmatrix} \tag{3.11}$$

with the matrix components being

$$\delta T_{11}^{\mathcal{NC}} = T_{12}^{\mathcal{NC}} \delta\theta - T_{21}^{\mathcal{NC}} \delta\Omega + T_{31}^{\mathcal{NC}} \sin\omega \delta i \tag{3.12}$$

$$\delta T_{21}^{\mathcal{NC}} = T_{22}^{\mathcal{NC}} \delta\theta + T_{11}^{\mathcal{NC}} \delta\Omega - T_{31}^{\mathcal{NC}} \cos\omega \delta i \tag{3.13}$$

$$\delta T_{21}^{\mathcal{NC}} = T_{32}^{\mathcal{NC}} \delta\theta + \sin\theta \cos i \delta i \tag{3.14}$$

When these quantities are substituted into eq. 3.11 the deputy position can be written in terms of orbit element differences as

$$^{\mathcal{C}}\boldsymbol{r}_d = \begin{pmatrix} R + \delta R \\ 0 \\ 0 \end{pmatrix} + R \begin{pmatrix} 0 \\ \delta\theta + \delta\Omega \cos i \\ -\cos\theta \sin i \delta\Omega + \sin\theta \delta i \end{pmatrix} \tag{3.15}$$

and if the radius R is expressed as a function of the given quantities (eq. 3.1)

$$R = \frac{a\left(1 - q_1^2 - q_2^2\right)}{1 + q_1 \cos\theta + q_2 \sin\theta} \tag{3.16}$$

its variation can be calculated as

$$\delta R = (R/a)\,\delta a + (V_r/V_t)\,R\delta\theta - (R/p)\,(2aq_1 + R\cos\theta)\,\delta q_1 - (R/p)\,(2aq_2 + R\sin\theta)\,\delta q_2 \tag{3.17}$$

where radial and transversal velocity components V_r and V_t are defined as

$$V_r = \dot{R} = (h/p)\,(q_1\sin\theta - q_2\cos\theta) \tag{3.18}$$

$$V_t = R\dot{\theta} = (h/p)\,(1 + q_1\cos\theta + q_2\sin\theta) \tag{3.19}$$

with h being the chief orbit momentum and p chief orbit semilatus rectum. In this way it is finally possible to obtain LVLH Cartesian components x, y and z of the deputy satellite function of orbital elements difference:

$$x = \delta R \tag{3.20}$$

$$y = R\,(\delta\theta + \cos i\delta\Omega) \tag{3.21}$$

$$z = R\,(\sin\theta\delta i - \cos\theta\sin i\delta\Omega) \tag{3.22}$$

With these relations it is possible to describe, for example, the relative orbit of two satellites in formation flight as a function of the true anomaly (or the true latitude) when initial orbital elements of the satellites are assigned. Next figures present an example of application of these relations: in this case chief and deputy satellites orbital elements are

$$\boldsymbol{e}_c = \begin{pmatrix} 7555\ km \\ 0.03 \\ 48\pi/180\ rad \\ 20\pi/180\ rad \\ 10\pi/180\ rad \\ 0\pi/180\ rad \end{pmatrix}$$

$$\boldsymbol{e}_d = \begin{pmatrix} 7555\ km \\ 0.03095316 \\ 48\pi/180\ rad \\ 20.1\pi/180\ rad \\ 10.1\pi/180\ rad \\ 0\pi/180\ rad \end{pmatrix}$$

so that their orbital elements differences are

$$\delta\boldsymbol{e} = \begin{pmatrix} 0\ km \\ 0.00095316 \\ 0\ rad \\ 0.1\pi/180\ rad \\ 0.1\pi/180\ rad \\ 0\ rad \end{pmatrix}$$

Both numerical integration and approximated orbit propagation has been performed and the results are compared here. In figure 3.1 the relative orbit three–dimensional plot of is presented, while in figure 3.2 the trend for each Cartesian component is reported. In both figures there are the numerical (dotted line) and the approximated (solid line) results, but it is quite clear that they are so close that is substantially impossible to distinguish one from the other. For this reason, in figure 3.3 the relative error for each of the three components is reported, the difference between numerical and approximated result is divided by the relative orbit radius $\rho(\nu)$. The error is less than one percentage point.

The approach main limit is related with the impossibility to propagate relative orbits in case orbital perturbation acting on satellites needs to be taken into account. In this case, in fact, numerical integration is mandatory. Next part of this chapter is dedicated to find a way to overcame this relevant issue.

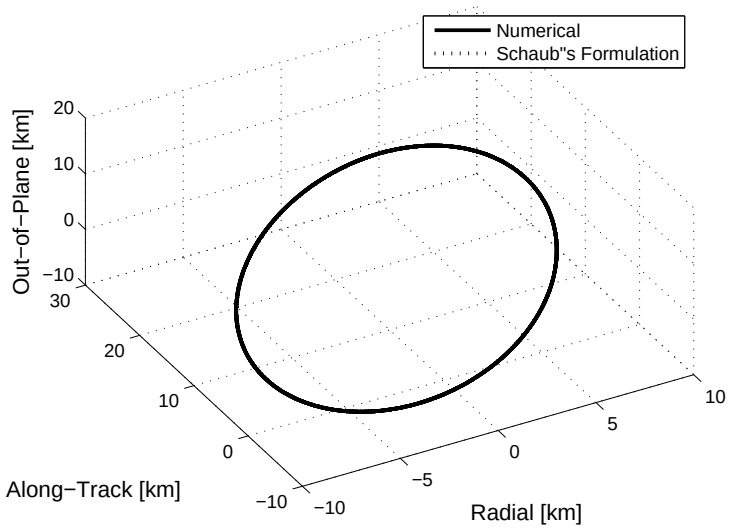

Figure 3.1: Chief–Deputy relative orbit, three–dimensional plot

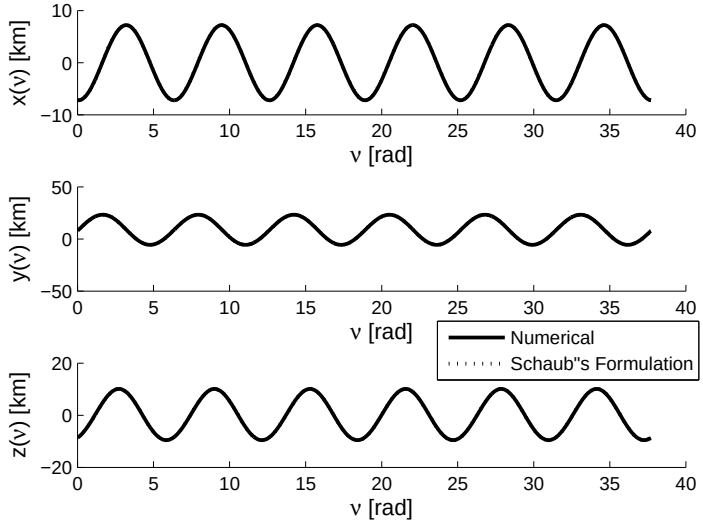

Figure 3.2: Chief–Deputy relative orbit components function of ν

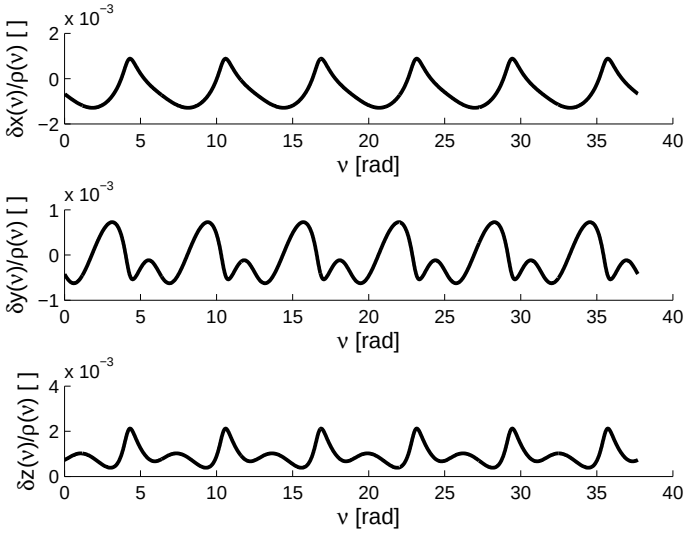

Figure 3.3: Chief–Deputy relative orbit components relative error

3.2 Perturbation Method and Schaub's Formulation

Schaub's formulation uses classical orbital parameters differences to derive the whole relative orbit propagation using the true anomaly ν as independent variable. But this approach can be applied only in case orbital parameters of both satellites are analytically known at every propagation step. This is impossible when dealing with perturbed orbit, but it appears to be a suitable setting to apply perturbative expansions derived in the previous chapter. In fact the independent variable is the same (i.e. the true anomaly ν) and by means of the approximated expansion for both satellites it is possible to know the variation of each orbital element in every step forward performed in the true anomaly when the orbit is propagated.

Actually the process is a little bit more complicated: in fact in order to derive the correct perturbed orbital element of the deputy satellite, its actual increment in true anomaly needs to be computed, while to apply Schaub's formulation just the chief increment in true longitude is needed. In order to derive the deputy increment in true anomaly the time equation has to be used: the chief satellite time of flight must be the same of the deputy one, in this way, solving these Kepler problem, it is possible to know which is the correct deputy true anomaly, and to compute also its perturbed orbital elements.

Summarizing in steps the whole approach developed in this chapter it is:

- Schaub's formulation gives the relative orbit radius between two spacecrafts in LVLH components as a function of their orbital elements and true anomaly of the chief satellite $[x(\nu_c), y(\nu_c), z(\nu_c)] = f(\boldsymbol{e}_c, \boldsymbol{e}_d, \nu_c)$;
- Perturbative expansions give the variation of a spacecraft orbital elements caused by a perturbation acting on it as a function of the acceleration magnitude caused by the perturbation, its orientation and true anomaly $\boldsymbol{e}_i = f(\varepsilon_i, \alpha_i, \beta_i, \nu_i)$;
- Merging the two approaches it is possible to obtain a simple description of the relative orbit radius between two spacecrafts in LVLH components when they are subject to orbital perturbations as a function of the acceleration magnitude (for both spacecrafts), its orientation (for both spacecrafts) and chief satellite true anomaly $[x(\nu_c), y(\nu_c), z(\nu_c)] = f(\varepsilon_c, \alpha_c, \beta_c, \varepsilon_d, \alpha_d, \beta_d, \nu_c)$

This last relation appears to be really interesting, in fact it allows to describe, in an approximated way, the relative motion of two satellites even when they are subject to orbital perturbations without the use of numerical integration on the differential equation of motion. Major limitations are the perturbation magnitude and orientation must be considered constant, at least on intervals.

3.3 Results

In what follows a case study on the JAXA reference model 2003 is presented. First of all the perturbation magnitude must be evaluated. Considering data reported on [23] about the dimensions of the concept it is possible to obtain a numerical reference value. Having a satellite surface of $S = 2.5 \cdot 3.5 = 8.75\ km^2$ and a mass of $m = 1000\ ton$ with a solar radiation pressure at $1\ AU$ from the Sun of $p_{SR} = 9.15\ N/km^2$ the perturbing acceleration is

$$\varepsilon = \frac{p_{SR} S}{m} \cong 8 \cdot 10^{-8}\ m/s^2$$

Its direction has been assumed constant and equal for both the satellites, with $\alpha_c = \alpha_d = 90\ deg$ and $\beta_c = \beta_d = 10\ deg$. The reason of this choice is mainly related to the will to obtain a closed reference orbit. Initial orbital

parameters are set as

$$\boldsymbol{e}_c = \begin{pmatrix} 7555\ km \\ 0.03 \\ 48\pi/180\ rad \\ 20\pi/180\ rad \\ 10\pi/180\ rad \\ 0\pi/180\ rad \end{pmatrix}$$

$$\boldsymbol{e}_d = \begin{pmatrix} 7555\ km \\ 0.03095316 \\ 48\pi/180\ rad \\ 20.1\pi/180\ rad \\ 10.1\pi/180\ rad \\ 0\pi/180\ rad \end{pmatrix}$$

and the simulation is performed for one entire chief orbit.

Three evaluations of the relative orbit as been computed: one accurate numerical taken as the reference value (it is reported with a dotted black line in the following figures) and two evaluations with the approximated relations. As said in the dedicated chapter the approximated time equation contains some terms that needs integrals numerical evaluation, it improves the accuracy but it also requires more computational time. So two different versions of the time equation have been used: the first one is the complete first order formulation (black solid line), while the second one takes into account only analytical terms (red solid line), i.e. it is less accurate but faster.

In figure 3.4 it is possible to see the three–dimensional plot of the relative orbit, while in figure 3.5 the three components of the orbit radius are reported as a function of the time of flight. It is almost impossible to distinguish between the three lines, so that in figure 3.6 relative errors of the two approximated relations with respect to the numerical evaluation are reported. It is clear that for one simulated orbit the errors of the x and z component are under one percentage point, while for the y component it is a little bit higher even if still under the 3%. It is also important to be noticed

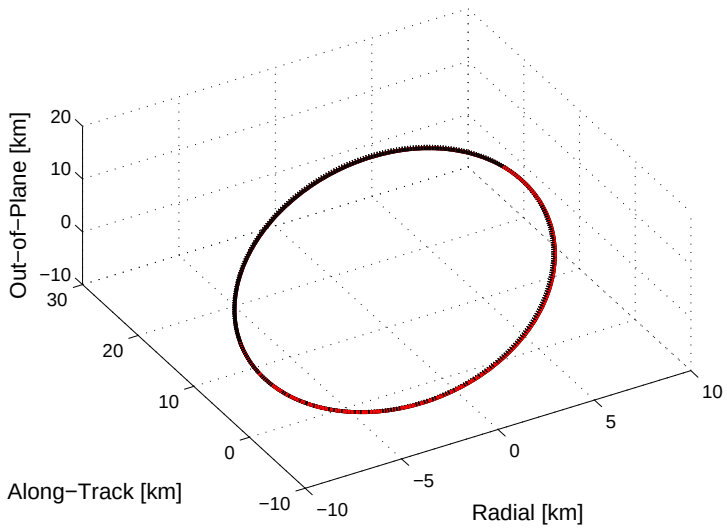

Figure 3.4: Relative orbit, three–dimensional plot

that the error of the approximated solution with only analytical terms, that is less accurate, is really near to the other solution, only for the third component it grows in a significant manner after a half revolution. It gains even greatest importance when this fact is compared with the final two figures: in fig. 3.7 is reported the computational time ratio between the approximated complete relation and the accurate numerical evaluation while in fig. 3.8 the same quantity is referred to the approximated relation with only analytical terms. In the first case the approximated relations are faster than the numerical ones, but with a CPU time saving of about 50%. On the other hand, in the second case we have an algotithm which is approximately 1500 times faster than the numerical one.

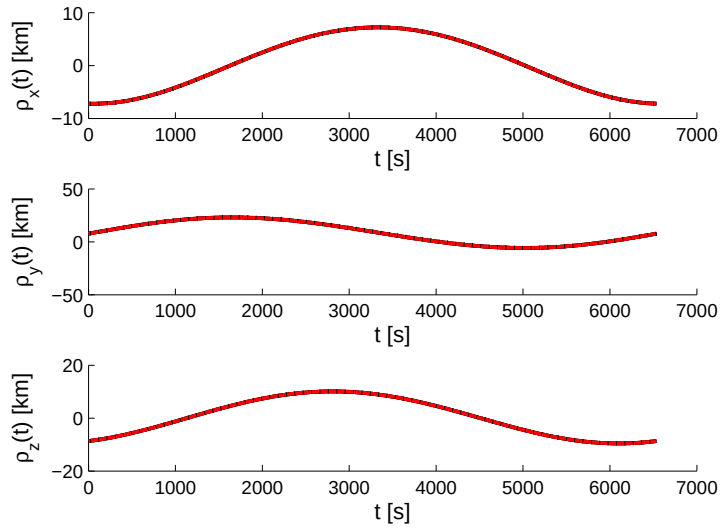

Figure 3.5: Orbit components function of time of flight

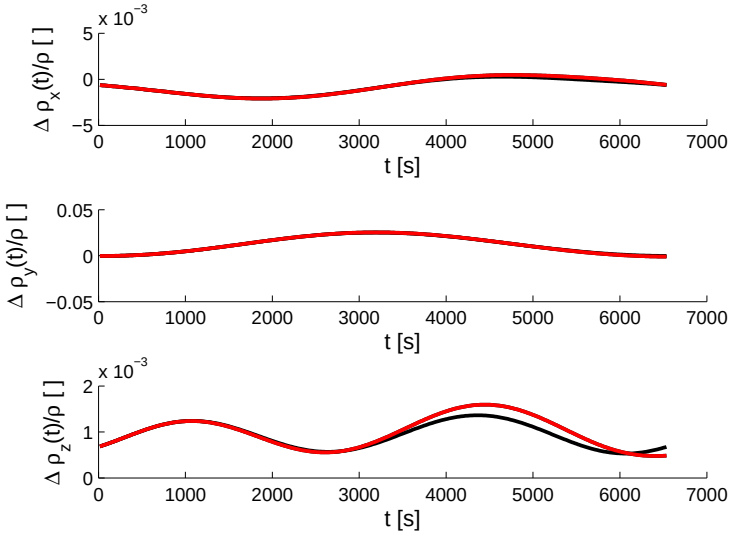

Figure 3.6: Orbit components relative error function of time of flight

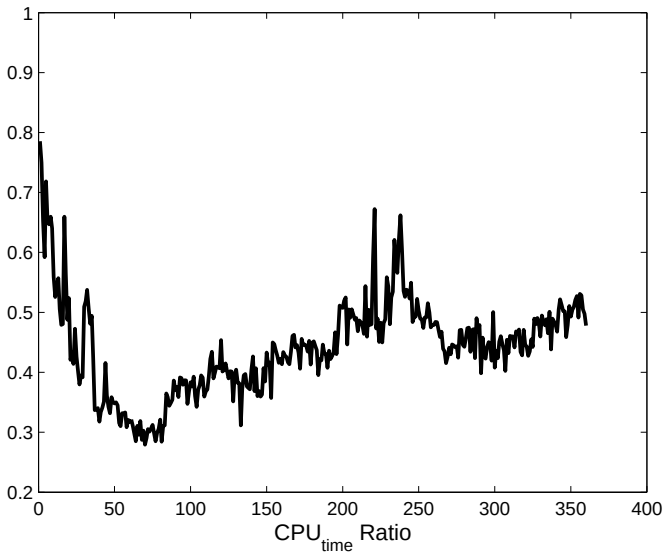

Figure 3.7: CPU time ratio first case

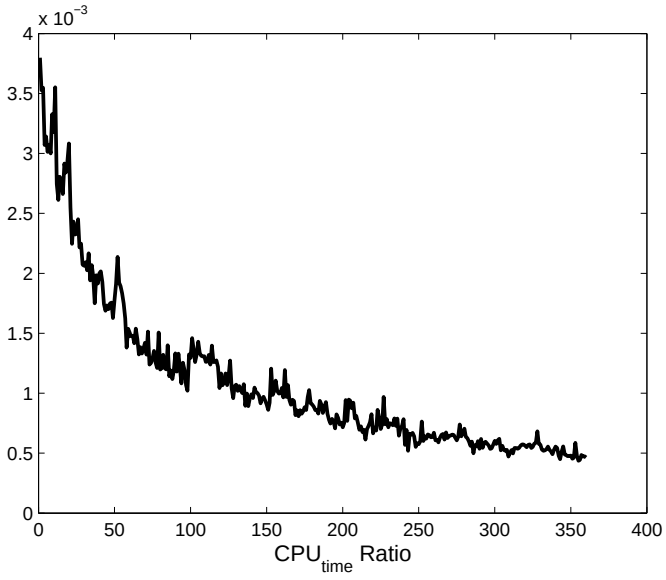

Figure 3.8: CPU time ratio second case

This page intentionally left blank

Chapter 4

SPS Finite Element Model

In this chapter the Finite Element Model used to describe the SPS structure will be presented. As said in previous chapters, the considered concept, JAXA 2003 reference concept, is composed by three different satellites [8][23]: two reflectors/collectors which have to direct solar rays into the central satellite, equipped with solar cells and a microwave antenna to beam the power down to the Earth rectenna on the surface. While the reflectors/collectors have a circular shape, the central satellite is rectangular, in addition the latter satellite need to be accurately pointed in order to transmit the power minimizing losses. Accurate attitude control is needed in order to assure the correct orientation and, given the dimensions of these satellites typology (square kilometers), it is clear that a vibration control would be inevitable.

Complex systems, like satellites, are really difficult, if not impossible, to be described by means of infinite–dimensional models which can instead be applied on simple systems. As it will be shown in the next chapter there are different ways to study complex systems, one of these is Finite Element Method. This technique, which is well developed in the stress–strain analysis for structural studies, can be successfully applied in structural dynamics too. It is for sure the most straightforward to be applied and in the results interpretation.

4.1 FEM preliminary discussion

Speaking in general sense, Finite Element Method is a mathematical technique that allows to solve complex problems. These methods have been developed in the second half of the XX century when numerical methods started to appear as an important mean to obatain accurate results for complex systems. The starting point for structural studies is represented by some

important relations (these few lines will be limited to the linear case):

1. Indefinite equilibrium equations: these are partial differential equations that link the stress tensor to the external forces, they can be easily derived studying the equilibrium of an infinitesimal cube.

2. Geometrical relations: these are partial differential equations that link the deformation tensor to the physical displacements, they can be easily derived looking at the geometrical relations for an infinitesimal cube.

3. Constitutive relations or Hooke Law: it is the law that describe the (usually elastic) relation between the stress and the deformation tensor.

This fundamentals relations form a system of partial differential equations that describe how external forces acting on an object would modify or act on its spatial geometry. In the general case of complex geometries they cannot be solved analitically. Looking at the problem from a strictly mathematical point of view, FEM can be described as a method to find a solution to a slightly different (weak) problem, that is a proper transformation of the previous one. It can be more straightforward to see things in a different way: thanks to the virtual work principle, in fact, the previous problem can be revisited and seen like an application of the first thermodynamic principle: the work done by external forces must be equal to the one done by the internal stresses. It is not so simple to accurately show every mathematical step that allow to reach the final elegant result, but the main steps can be summarized as follows:

1. Starting from the constitutive relations, stresses can be written as a funtion of deformations.

2. A displacement model has to be chosen. This is the most difficult part, in fact here the scientist has to immagine and choose which physical phenomena are important in the considered structure behaviour, and to describe them accurately. Usually this task is not something everyone can do, and literature models are used (Kirchoff plate is an example). Here is where deformations are written as functions of external displacements.

3. Finally, discretization takes place. Since only finite dimensional systems can be addressed in numerical methods, external (infinite) displacements need to be properly related with the displacements of some, peculiar, points of the structure. This task is performed using the so called shape functions, that are the relations that describe the structure displacements in terms displacements of some particular points.

At the end of this process (that is far more complicate than it seems, in fact displacement models or shape function are a very large topic and a huge research field), a very elegant formulation for the static equilibrium problem is reached:

$$K\vec{x} = \vec{F}$$

where K is the so called stiffness matrix, $\vec{x}$ are the displacements and $\vec{F}$ external forces. The stiffness matrix is the output of all the process described in the previous steps, inside it are contained all the choices made in chosing the constitutive relation (material behaviour), displacement model (structure behaviour) and shape functions (discretization). As stated before, this was the case of a static equilibrium problem, in case a dynamic problem is faced, accelerations (second derivative in time) need to be considered. Derivation is not so different, time derivative does not influence the very same approach described for the static case, so the output will be an additional matrix M, the so called mass matrix, that is added to the previous formulation as follows:

$$M\ddot{\vec{x}} + K\vec{x} = \vec{F}$$

The Mass matrix takes into account the inertial part of the problem. An additional observation can be useful: who is familiar with second order mechanical systems dynamics, would have noted that there are no damping terms, terms related with the velocity (first derivative of displacements). In fact, the formal modelization of this phenomenon is not so simple, it deals with non conservative energy transformation and so it cannot be treated in the same way. The usual way to deal with this aspect, as it will be shown later, is to obatain the damping matrix C, as a function of the other two, M and K.

These concepts will be used in what follows to simulate a complex structure, describing its vibrational (second order) dynamics by means of these three matrices: M, C and K, this is why a FEM model is needed.

4.2 FEM application

In what follows the principal steps for the structure modeling are listed and described, they are:

- geometry choice;
- finite element characteristics choice;
- input data;

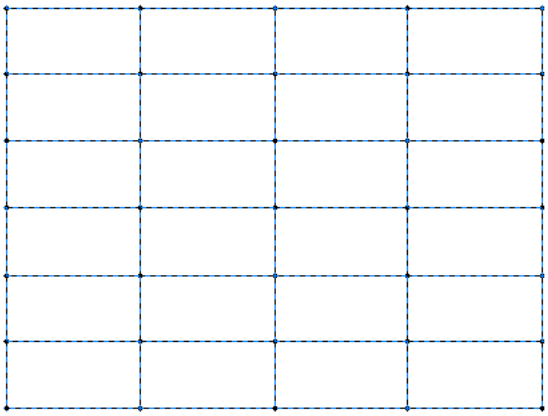

Figure 4.1: SPS FEM Geometry

- output data.

Geometry

Since the structure thickness is very small if compared with the other two dimensions (order of tens of meters vs kilometers[8][23]) it is justified to model the SPS like a two–dimensional system. Various papers in literature about different SPS concept agree that the need to limit the structure weight suggest a frame structure, i.e. a structure composed by various beams. For this reason the adopted geometry has been a two–dimensional rectangular beam frame (see fig. 4.1). The whole structure is created by means of a connectivity matrix connecting different beams, taking into account their orientation in space. Every rectangle composed by four beams (two horizontal and two vertical) will be named 'sub–structure'. Every beam has the same inertia moments, material and section area. The mesh will be regular and isometric (same number of element per each beam) and only isotropic and homogeneous materials will be considered.

Finite Element

The structure has to withstand loads in every direction, both in–plane and out–of–plane forces and torques. For this reason a three–dimensional beam element has been chosen, so that six degrees of freedom are present at each node, three displacements and three rotations. Each beam is capable, other than to bend orthogonally with respect to its axis, also to resist to torsional torques.

Input Data

In order to completely describe the structure the following inputs are needed:

- n_{row}: number of sub–structure per row;
- n_{column}: number of sub–structure per column;
- section properties: area A and three inertia moments I_y, I_z and J (polar moment of inertia), where x is the beam axis;
- material properties: density ρ, Young modulus E and shear modulus G (or Poisson modulus ν);
- n_{el}: number of elements per beam;
- structure dimensions: L_x x–length and L_y y–length;
- constraints matrix V: it is a matrix which simply contains the number of the constrained displacements, thus if it is a empty matrix the structure is unconstrained (this will be the considered case).

Output Data

All the structure is described just by means of two matrices: the mass matrix M and the stiffness matrix K. These two quantities will be two of three outputs of the FEM model, the last one being the load matrix D which will be used to add the control forces/torques to the system. In this way no structural damping would be taken into account in the structure dynamics, usually the damping matrix C is obtained as linear combination of the other two, so that

$$C = c_K K + c_M M$$

where the coefficients c_K and c_M are usually evaluated by means of experiments.

4.3 FEM implementation

The FEM software implementation can be described by means of different steps:

- All inputs values are assigned by the user: n_{row}, n_{column}, n_{el}, L_x, L_y, A, I_y, I_z, J, ρ, E, G;

- With n_{row}, n_{column} and n_{el} the connectivity matrix B can be automatically created. This matrix has a number of rows equal to the number of total beam elements in the structure, and three columns: in the first and second columns are listed the starting and ending node for the given beam element (i.e. the given i-th row) and the third column gives the orientation of the beam: 1 if horizontal and 2 if vertical.

- With L_x, L_y, A, I_y, I_z, ρ, E, G and the Connectivity Matrix B both mass M and stiffness K matrices can be automatically created. It can be done quite easily starting from the element mass and stiffness matrices M_{el} and K_{el} and putting them into the main matrices following the indication given by the connectivity matrix which lists the linked nodes. The element matrices are standard for a single beam element once the shape functions are assigned (i.e. the model is chosen), in this case element matrices described in [17] has been used. They are obviously 12×12 matrices, since each element has two nodes and each node has six degrees of freedom:

$$K_{el} = \begin{bmatrix}
\frac{AE}{L_i} & 0 & 0 & 0 & 0 & 0 & -\frac{AE}{L_i} & 0 & 0 & 0 & 0 & 0 \\
 & \frac{12EI_z}{L_i^3} & 0 & 0 & 0 & \frac{6EI_z}{L_i^2} & 0 & -\frac{12EI_z}{L_i^3} & 0 & 0 & 0 & \frac{6EI_z}{L_i^2} \\
 & & \frac{12EI_y}{L_i^3} & 0 & -\frac{6EI_y}{L_i^2} & 0 & 0 & 0 & \frac{12EI_y}{L_i^3} & 0 & -\frac{6EI_y}{L_i^2} & 0 \\
 & & & \frac{GJ}{L_i} & 0 & 0 & 0 & 0 & -\frac{GJ}{L_i} & 0 & 0 & \\
 & & & & \frac{4EI_y}{L_i} & 0 & 0 & 0 & \frac{6EI_y}{L_i^2} & 0 & \frac{2EI_y}{L_i} & 0 \\
 & & & & & \frac{4EI_z}{L_i} & 0 & -\frac{6EI_z}{L_i^2} & 0 & 0 & 0 & \frac{2EI_z}{L_i} \\
 & & & & & & \frac{AE}{L_i} & 0 & 0 & 0 & 0 & 0 \\
 & & & & & & & \frac{12EI_z}{L_i^3} & 0 & 0 & 0 & -\frac{6EI_z}{L_i^2} \\
 & & & & & & & & \frac{12EI_y}{L_i^3} & 0 & \frac{6EI_y}{L_i^2} & 0 \\
 & & sy. & & & & & & & \frac{GJ}{L_i} & 0 & 0 \\
 & & & & & & & & & & \frac{4EI_y}{L_i} & 0 \\
 & & & & & & & & & & & \frac{4EI_z}{L_i}
\end{bmatrix}$$

$$M_{el} = \frac{\rho A L_i}{210} \begin{bmatrix} 70 & 0 & 0 & 0 & 0 & 0 & 35 & 0 & 0 & 0 & 0 & 0 \\ & 78 & 0 & 0 & 0 & 11L_i & 0 & 27 & 0 & 0 & 0 & -7.5L_i \\ & & 78 & 0 & -11L_i & 0 & 0 & 0 & 27 & 0 & 7.5L_i & 0 \\ & & & 70h & 0 & 0 & 0 & 0 & 0 & -35h & 0 & 0 \\ & & & & 2L_i^2 & 0 & 0 & 0 & -7.5L_i & 0 & -1.5L_i^3 & 0 \\ & & & & & 2L_i^2 & 0 & 7.5L_i & 0 & 0 & 0 & -1.5L_i^2 \\ & & & & & & 70 & 0 & 0 & 0 & 0 & 0 \\ & & & & & & & 78 & 0 & 0 & 0 & -11L_i \\ & & & & & & & & 78 & 0 & 11L_i & 0 \\ & & sy. & & & & & & & 70h & 0 & 0 \\ & & & & & & & & & & 2L_i^2 & 0 \\ & & & & & & & & & & & 2L_i^2 \end{bmatrix}$$

where

$$h = \frac{J}{A}$$

while the main matrices will be $6n_{nodes} \times 6n_{nodes}$ where n_{nodes} depends on n_{row}, n_{column} and n_{el}.

4.4 Results

In this section some results are presented. As it will be shown in Chapter 6 one of the initial steps to be performed when the structure dynamics is studied is the evaluation of its modal shapes. It can be done simply by solving the eigenvalue problem using mass and stiffness matrix: eigenvalues are directly linked to structure natural frequencies while the associated eigenvectors are the corresponding modal shapes. Here after some figures are presented with first six modal shapes, it has to be underlined that in case the constraints matrix V is empty (i.e. the structure is unconstrained) six rigid motions arise in the modal shapes, so the significant values would start from the seventh eigenvector on.

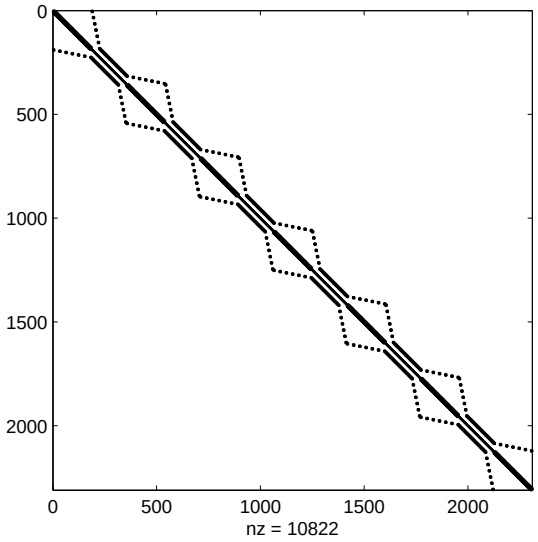

Figure 4.2: Mass and stiffness matrices population

These results were obtained with unitary values for all the material inputs (A, I_y, I_z, J, ρ, E, G) since the aim is just to show how the software works. Natural frequencies numerical values depend on these characteristics, so that their value presented here has not physical significance. It scales with material input values, but its progression is obviously still valid to put modal shapes in the proper real order. Remaining parameters have been chosen as $n_{row} = 6$, $n_{column} = 6$ and $n_{el} = 5$. Figure 4.2 presents how mass and stiffness matrices are populated.

Next figures presents first six eigenvectors, undeformed shape is depicted with blue color, while the deformed one is in black:

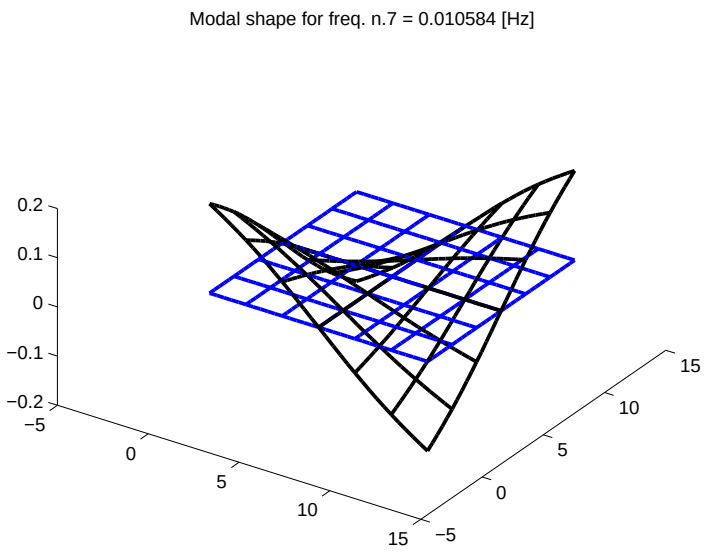

Figure 4.3: First modal shape

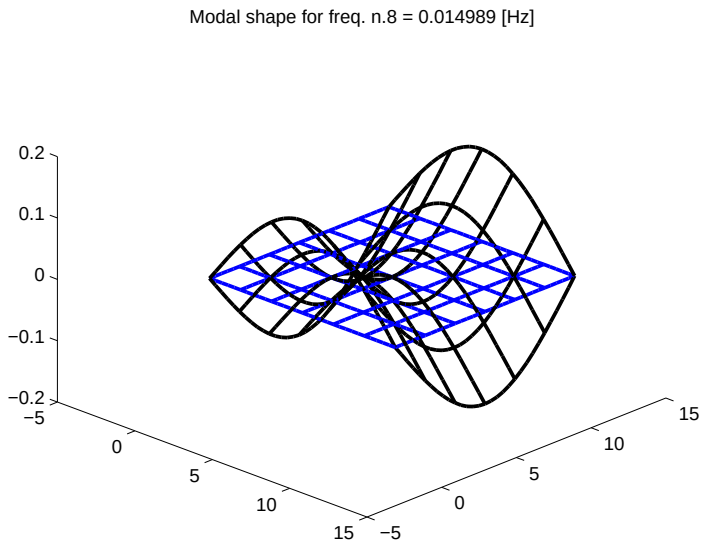

Figure 4.4: Second modal shape

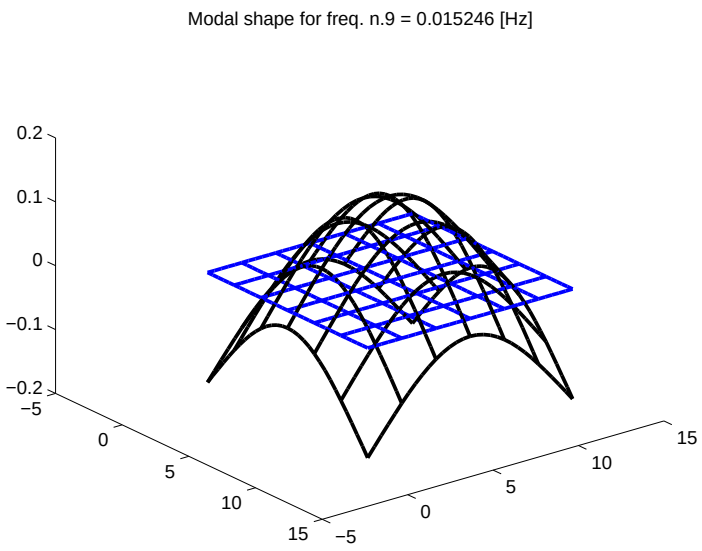

Figure 4.5: Third modal shape

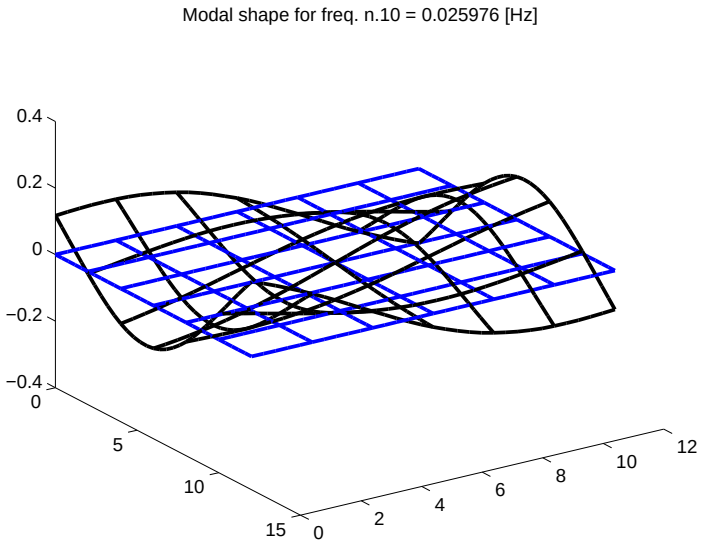

Figure 4.6: Fourth modal shape

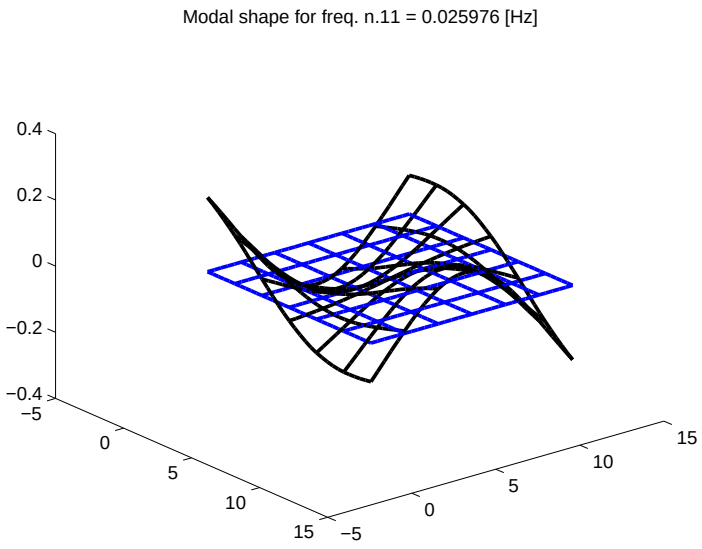

Figure 4.7: Fifth modal shape

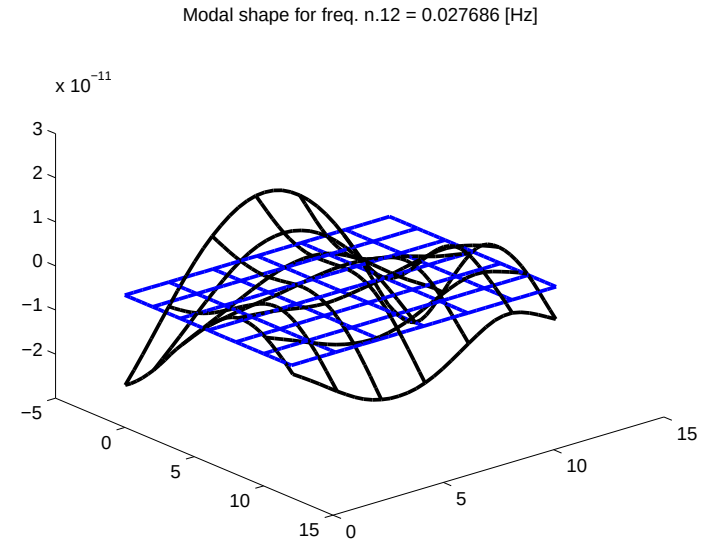

Figure 4.8: Sixth modal shape

This page intentionally left blank

Chapter 5

Optimization Methods Fundamentals

In this chapter a brief general overview on optimization methods is given, first of all there is a classification of optimization techniques and then the description of each category, but only Evolutionary Methods are treated with some details, since this category will be applied in the actuator placement problem.

5.1 Optimization Problem Formalization

The common formalization[3] for a generic optimization problem presents a functional

$$J = \phi(\boldsymbol{x}_0, \boldsymbol{x}_f, t_0, t_f) + \int_{t_0}^{t_f} \Phi\left(\boldsymbol{x}, \dot{\boldsymbol{x}}, t\right) dt \tag{5.1}$$

which is a measure of the system performance (it is also called 'performance index'), where

- t si the independent variable;
- $\boldsymbol{x}$ are state variables (n–component vector);
- $\boldsymbol{u}$ are control variables (m–component vector);
- $\dot{\boldsymbol{x}} = dx/dt = \boldsymbol{f}\left(\boldsymbol{x}, \boldsymbol{u}, t\right)$ are state equations (n–component vector of differential equations);
- $\boldsymbol{\psi}\left(\boldsymbol{x}_0, \boldsymbol{x}_f, t_0, t_f\right) = 0$ are boundary conditions (q–component vector of algebraic equations, $q \leq n + 2$).

The target is to find the so called extremal path $\boldsymbol{x}(t)$ and the corresponding optimal control law $\boldsymbol{u}(t)$ satisfying the state equations and the constraints to maximize (or minimize, it is the same[1]) the functional (i.e. performance index). This is the so called 'Optimal Control Problem'.

Different methods can be used to solve this problem, they are usually grouped as follows

- Indirect Optimization Methods;
- Direct Optimization Methods.
  - Gradient Based Methods;
  - Evolutionary Methods;

Each category has its peculiarity which fits some kind of problems better than others, their description is given in next sections.

5.2 Indirect Optimization Methods

These methods are based on calculus of variations, so that they can face continuous problems avoiding the problem of the discretization. As their name suggest, they obtain the condition for the performance index maximization without evaluating it directly. In order to work on an unconstrained problem the augmented performance index is built

$$J^* = J + \boldsymbol{\mu}^T \boldsymbol{\psi} + \int_{t_0}^{t_f} \left[\boldsymbol{\Phi} + \boldsymbol{\lambda}^T \left(\boldsymbol{f} - \dot{\boldsymbol{x}} \right) \right] dt \tag{5.2}$$

where $\boldsymbol{\lambda}$ are the adjoint variables and $\boldsymbol{\mu}$ are the adjoint constants; in this way, when the constraints are satisfied

$$J^* = J$$

In case of inequality constraints the user has to choose which are active (i.e. these will become equality constraints) and which are not; this choice has to be verified at the end of the process.

[1] Minimize the time t can be seen as maximizing $-t$.

In order to obtain the optimality conditions one has to analyze the first variation of the augmented performance index, so

$$\begin{aligned} dJ^* &= \left(\frac{\partial\phi}{\partial t_f} + \boldsymbol{\mu}^T\frac{\partial\boldsymbol{\psi}}{\partial t_f} + H_f\right)dt_f + \\ &+ \left(\frac{\partial\phi}{\partial t_0} + \boldsymbol{\mu}^T\frac{\partial\boldsymbol{\psi}}{\partial t_0} - H_0\right)dt_0 + \\ &+ \left(-\boldsymbol{\lambda}_f^T + \frac{\partial\phi}{\partial\boldsymbol{x}_f} + \boldsymbol{\mu}^T\frac{\partial\boldsymbol{\psi}}{\partial\boldsymbol{x}_f}\right)d\boldsymbol{x}_f + \\ &+ \left(\boldsymbol{\lambda}_0^T + \frac{\partial\phi}{\partial\boldsymbol{x}_0} + \boldsymbol{\mu}^T\frac{\partial\boldsymbol{\psi}}{\partial\boldsymbol{x}_0}\right)d\boldsymbol{x}_0 \\ &+ \int_{t_0}^{t_f}\left[\left(\frac{\partial H}{\partial\boldsymbol{x}} + \dot{\boldsymbol{\lambda}}^T\right)\delta\boldsymbol{x} + \frac{\partial H}{\delta\boldsymbol{u}}\delta\boldsymbol{u}\right]dt \end{aligned}$$

in the maximum point the first variation must be zero. Isolating each term one obtains: two boundary conditions for optimality ($2n$ algebraic equations at initial and final point)

$$-\boldsymbol{\lambda}_f^T + \frac{\partial\phi}{\partial\boldsymbol{x}_f} + \boldsymbol{\mu}^T\frac{\partial\boldsymbol{\psi}}{\partial\boldsymbol{x}_f} = 0; \quad \boldsymbol{\lambda}_0^T + \frac{\partial\phi}{\partial\boldsymbol{x}_0} + \boldsymbol{\mu}^T\frac{\partial\boldsymbol{\psi}}{\partial\boldsymbol{x}_0} = 0 \tag{5.3}$$

two transversality conditions (2 algebraic equations at initial an final time)

$$\frac{\partial\phi}{\partial t_f} + \boldsymbol{\mu}^T\frac{\partial\boldsymbol{\psi}}{\partial t_f} + H_f = 0; \quad \frac{\partial\phi}{\partial t_0} + \boldsymbol{\mu}^T\frac{\partial\boldsymbol{\psi}}{\partial t_0} - H_0 = 0$$

one set of differential equations for the adjoint variables, Euler–Lagrange equations (n differential equations)

$$\dot{\boldsymbol{\lambda}} = -\frac{\partial H}{\partial\boldsymbol{x}}^T$$

and one set of equations for the optimal control (m algebraic equations for the control variables)

$$\frac{\partial H}{\partial\boldsymbol{u}}^T = 0$$

In this way the Optimal Control Problem becomes a Boundary Value Problem, which is completely defined and all the variable trends in time can be determined numerically solving the differential equations. Besides this simple considerations there are also other kind of evaluations, like the controllability condition, deviations from optimum and the second variation evaluation, but here they are not taken into account. Main problems for these methods are the difficulty to solve the Boundary Value Problem, the possibility to find suboptimal solutions instead of globally optimal ones, and the convergence dependence on the initial guess.

5.3 Direct Methods

In these methods controls and states are approximated by means of polynomial or piecewise functions over small intervals, once these approximations are substituted inside the optimal control problem formulation it becomes a classic Linear or Non Linear Problem Optimization where the functional J become the 'cost function', i.e. the problem and the solution are no more continuous. It is unlikely, in advanced engineering, to find Linear Optimization Problems (usually solved by means of the Simplex Algorithm), so that only Non Linear Optimization Problems (i.e. Non Linear Programming - NLP) are taken into account in what follows.

Two different types of algorithms are grouped in direct methods:

- Gradient Based Algorithms
- Evolutionary Algorithms

5.3.1 Gradient Based Algorithms

These methods can deal with a great number of variables, the NLP is the maximization of the performance index $\phi(x)$ respecting the constraints

$$\boldsymbol{c}(\boldsymbol{x}) \geq 0$$

where

- $\boldsymbol{x}$ is a n–component vector of variables, $\boldsymbol{x}^T = [x_1, x_2, ..., x_n]$;
- $\boldsymbol{c}$ is a m–component vector of constraints, $\boldsymbol{c}^T = [c_1, c_2, ..., c_m]$, and m maybe larger than n.

There are two main sub–categories for these methods:

- Simple Gradient Methods;
- Sequential Quadratic Programming (SQP).

Simple Gradient Methods

In these methods the gradient is evaluated perturbing a feasible solution of the problem, the new solution is found moving along the gradient direction and the magnitude of this movement can be evaluated by means of different approaches in order to optimize the search. Anyway these methods suffer when the solution approaches a stationary point (so also when it is near to the problem solution), in fact in these regions the gradient value approaches zero and the direction of movement is no more defined.

Sequential Quadratic Programming

They are based on two approximations: one second–order approximation for the performance index and a first–order one for the constraints. The maximization problem solution is found by the solution of a succession of quadratic programming problems starting from a tentative solution $\boldsymbol{x}$. Assuming those approximations one can write

$$\phi(\boldsymbol{x}+\Delta\boldsymbol{x}) = \phi(\boldsymbol{x}) + \boldsymbol{g}^T\Delta\boldsymbol{x} + \frac{1}{2}\Delta\boldsymbol{x}^T[\boldsymbol{H}]\Delta\boldsymbol{x} \tag{5.4}$$

$$\boldsymbol{c}(\boldsymbol{x}+\Delta\boldsymbol{x}) = \boldsymbol{c}(\boldsymbol{x}) + [\boldsymbol{G}]\Delta\boldsymbol{x} \tag{5.5}$$

where the linear approximation for the gradient is adopted and

$$\boldsymbol{g}(\boldsymbol{x}+\Delta\boldsymbol{x}) = \boldsymbol{g}(\boldsymbol{x}) + [\boldsymbol{H}]\Delta\boldsymbol{x}$$

where $[\boldsymbol{H}]$ is the Hessian Matrix.

In order to treat the constraints the active set method can be used, it implies to consider the augmented performance index and to consider some constraints as active ($\boldsymbol{c}_a$) and some inactive ($\boldsymbol{c}_{na}$), so

$$\phi^* = \phi(\boldsymbol{x}) + \boldsymbol{\lambda}_a^T\boldsymbol{c}_a$$

and considering an increment one has

$$\phi^*(\boldsymbol{x}+\Delta\boldsymbol{x}) = \phi^*(\boldsymbol{x}) + \left(\boldsymbol{g}^T + \boldsymbol{\lambda}_a^T[\boldsymbol{G}_a]\right)\Delta\boldsymbol{x} + \frac{1}{2}\Delta\boldsymbol{x}^T[\boldsymbol{H}]\Delta\boldsymbol{x}$$

where the augmented Hessian is

$$[\boldsymbol{H}^*] = [\boldsymbol{H}] + \partial\left[\partial\left(\boldsymbol{\lambda}_a^T\boldsymbol{c}_a/\partial\boldsymbol{x}\right)^T\right]/\partial\boldsymbol{x}$$

and the conditions for optimality (for the given active set) are

$$\begin{aligned} \boldsymbol{g} + [G_a]^T\boldsymbol{\lambda}_a &= 0 \\ \boldsymbol{c}_a &= 0 \end{aligned}$$

and the addition of

$$\Delta\boldsymbol{x}^T[\boldsymbol{H}]\Delta\boldsymbol{x} < 0$$

for any variation $\Delta\boldsymbol{x}$ makes this set of condition sufficient for a maximum.

In general these conditions are not satisfied in a generic point so looking for a new point $\boldsymbol{x}+\Delta\boldsymbol{x}$, $\boldsymbol{\lambda}_a+\Delta\boldsymbol{\lambda}_a$ one can write

$$\begin{aligned} \boldsymbol{g}(\boldsymbol{x}) + [\boldsymbol{H}^*]\Delta\boldsymbol{x} + [\boldsymbol{G}_a]^T(\boldsymbol{\lambda}_a+\Delta\boldsymbol{\lambda}_a) &= 0 \\ \boldsymbol{c}_a(\boldsymbol{x}) + [\boldsymbol{G}_a]\Delta\boldsymbol{x} &= 0 \end{aligned}$$

where

$$\begin{aligned} \boldsymbol{g}(\boldsymbol{x}+\Delta\boldsymbol{x}) &= \boldsymbol{g}(\boldsymbol{x}) + [\boldsymbol{H}^*]\,\Delta\boldsymbol{x} \\ c_a(\boldsymbol{x}+\Delta\boldsymbol{x}) &= \boldsymbol{c}_a(\boldsymbol{x}) + [\boldsymbol{G}_a]\,\Delta\boldsymbol{x} \end{aligned}$$

and the previous equations can be rewritten in the most known form of the so called Karush - Kuhn - Tucker equations

$$\begin{bmatrix} [\boldsymbol{H}^*] & [\boldsymbol{G}_a]^T \\ [\boldsymbol{G}_a] & 0 \end{bmatrix} \begin{pmatrix} \Delta\boldsymbol{x} \\ \boldsymbol{\lambda}_a + \Delta\boldsymbol{\lambda}_a \end{pmatrix} = \begin{pmatrix} -\boldsymbol{g} \\ -\boldsymbol{c}_a \end{pmatrix}$$

and the search for the new point become an iterative procedure.

In the active set method one must not violate the inactive constraints so the step in the gradient direction towards the maximum point can be limited by a factor $\alpha \in [0,1]$ where

$$\alpha = min\left(\frac{-c_{na,i}}{\frac{\partial c_{na,i}}{\partial \boldsymbol{x}}\Delta\boldsymbol{x}}, 1\right)$$

when $\alpha < 0$ it is determined by $c_{na,i} = 0$ so the constrain must be added to the active set and when $\lambda_{a,i} < 0$ the corresponding constrain must be removed from the active set.

Until now the method can be regarded as a simple Newton's method, but there are some strategies that can be adopted to improve the algorithm; in particular this task is accomplished looking at the performance index in order to see if it is growing or not. A merit function is defined and in order to take into account the constraints it can be defined as

$$M = \phi + \boldsymbol{\lambda}_a^T \boldsymbol{c}_a - \frac{1}{2}\boldsymbol{c}_a^T\,[\boldsymbol{\rho}]\,\boldsymbol{c}_a$$

it is the augmented Lagrangian merit function, with ρ diagonal matrix with non negative terms: once $\Delta\boldsymbol{x}$ and $\Delta\boldsymbol{\lambda}$ are calculated the merit function is only a function of α so it is possible to chose the value of this parameter so that the merit function has a maximum; this method is the so called linear search. Another idea is the trust region method, it associates to the approximation of the performance index and the constraints a region of validity, so another equation comes out

$$\frac{1}{2}\Delta\boldsymbol{x}^T\Delta\boldsymbol{c} \leq \delta^2$$

KKT equations has to be modified introducing $[\boldsymbol{H}^*] - \tau\,[\boldsymbol{I}]$ instead of the augmented Hessian matrix.

For computational reasons linked to the calculus of the matrix and their factorization, can be useful to introduce slack variables, in this way one can transform inequality constraints in equality ones and force the inequality on the slack variables.

As said at the beginning of the section the problem must be discretized and split into finite intervals, for example if the time is the independent variable it must be split in $t_{i+1} - t_i = h_i$ where h_i is the integration step and an algebraic approximation must be introduced $\boldsymbol{y}_{i+1} = \boldsymbol{y}_i + \int_{t_i}^{t_{i+1}} \boldsymbol{f}(\boldsymbol{y}, t)\, dt$. This relation can be translated in terms of an integration scheme (Runge Kutta, Trapezoidal, Hermite Simpson, etc.). The usual way of solving these problems is tho use the Direct Transcription, it implies the use of a Multiple Shooting technique: the variables are the state and the controls at each node of any subinterval previously defined, supplementary equations are the matching conditions between the final point of one interval (which depends on the initial values on the node of that small sub element and the corresponding states and controls equations) and the initial one on the next element (see next figure for clearness). In order to evaluate the various matrix (gradient,

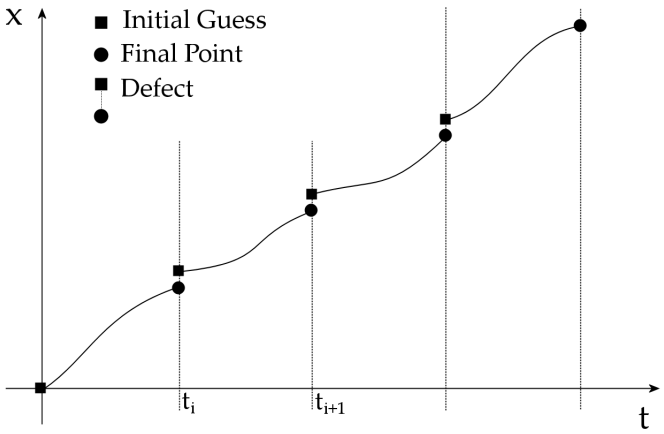

Figure 5.1: How multiple shooting works

Hessian, etc.) a perturbation on the initial parameters is introduced on the first integration step and then it is applied the recursive procedure.

5.3.2 Evolutionary Algorithms

These methods can only deal with a small number of variables (order of twenty). The basic principle of these methods is the emulation of physic natural phenomena. Each of them try to emulate one particular behavior of

nature in solving problems, it can be fishes or birds looking for food, natural selection of species, metallic crystal formation, etc. Hereafter three of them are described, they will be used in this study.

Genetic Algorithms

This category emulates the species natural selection: a set of individuals (the set of possible solutions) is randomly initialized. Each individual is then ranked by means of their performance index (a measure of the suitability for the given ambient, i.e. the optimization problem), there are various methods, the most common are:

- tournament: each individual is compared twice with others individuals, for each win it becomes a 'parent', if it loses both times it is discarded;
- roulette: the probability of selection is proportional to the performance index and 'parents' are chosen randomly with this probability distribution.

After this selection the best individuals, those in the 'parent group' are used to generate a new younger generation of solutions. Various reproduction methods can be adopted:

- single point crossover: the parents (i.e. the variables values which solve the problem) are mixed with a single intersection point, chosen randomly;
- double point crossover: the parents (i.e. the variables values which solve the problem) are mixed with a double intersection point, chosen randomly;
- weighted average: a weighted average of the parents (i.e. the variables values which solve the problem) is performed;

Then the algorithm is repeated until the stop condition is reached: it may be maximum number of iterations, minimum increment of performance index, etc.

There are some particular techniques which can be used to avoid to be stuck in a local maximum, and they are inspired by nature too: sometimes the worse individual are allowed to reproduce, sometimes there is a mass extinction of individuals and only few of the best survive, other times mutations are allowed, few of the best parents substitute the worse younger generated individuals (elitism), etc.

Particle Swarm Optimization

This algorithm simulates fishes or birds looking for food (the performance index maximum); a randomly initialized set of solutions is created and, instead of being replaced by other solutions, the individuals move around in the problem domain. Their motion is assumed to be similar to the one adopted by a flock of animals looking for food, in particular the acceleration of the individuals is given by two terms

$$v = v + c_1 k_1 \left(x_{P,best} - x\right) + c_2 k_2 \left(x_{G,best} - x\right)$$

the first is the personal–cognitive one (which points towards the area where the best value of performance index has been found during previous personal steps) and the second is the global–social one (which points towards the area where the best value of performance index has been found by the whole group). Personal position is then updated with the use of this velocity

$$y = x + v$$

Also in this case there are some strategies to improve the method, for example the choice of the acceleration coefficients and the choice to add an inertia related to the old velocity. Stop condition can be, as usual, maximum number of iterations, minimum increment of performance index, etc.

Differential Evolution

This method simulates the evolution too, a randomly generated set of solutions is created but in this case the process is more simple with respect to the genetic algorithm and the new population is created adding to one individual (it can be the best one or not) a component proportional (by means of some constants which can be used as degrees of freedom) to the difference between other two (or more than two) individuals:

$$y = x_1 + C \left(x_2 - x_3\right) + F \left(x_4 - x_5\right)$$

and the choice of x_i characterizes the method. In this way when the differences are big (at the beginning of the search) the domain is explored widely, while when the solutions are near the real optimum the search is performed only in that restricted area. As in previous cases the algorithm is stopped when a similar stop condition is met.

Other Methods

There are a lot of other methods:

- Ant Colony Optimization: it simulates the motion of ants and the way they interact in order to find the best path, it is very useful in vehicle routing problems;
- Simulated Annealing: it simulates the behavior of metallic crystals when starting from a hot temperature they are cooled down;
- Invasive Weed Optimization: it emulates the weed expansion looking for a suitable ambient;
- etc...

Since the initialization is done randomly and the search method is not based on standard optimality conditions these methods should not fall in sub–optimal solutions, but there is not the certainty of convergence, in fact the method performance is often evaluated looking to the percentage of times it converges (in test cases with known optimal solution) on the total runs.

Chapter 6

SPS Actuator Placement

In this chapter the second objective is addressed, the search for new and profitable ways to find an optimum actuator placement for flexible structures. First of all a brief introduction on some fundamental concepts in controllability and modal cost will be given. Then these instruments, together with those recalled about FEM modeling and optimization, will be merged and applied on the selected SPS concept, the JAXA SPS Reference Model 2003.

6.1 Controllability and Component Cost

The concept of controllability[1] is very relevant in the study of dynamical systems control. It is closely linked to the existence of a feasible control law which makes the closed loop stable with respect to the desired state or trajectory. Controllability measures the ability of a given actuator set to control chosen system states (for example some states important in the design process).

It is possible, and the scientific literature is a great resource of these studies, to transform this heuristic concept into mathematical terms. The first step is to state if the system is controllable or not. There are different ways to do so[13]: the controllability matrix $\mathcal{C}$, the controllability grammian W_c and different eigenvalues related quantities. Anyway this quantities give just the information if the system is controllable or not, they do not measure the system degree of controllability. This latter aspect can be really relevant because, in general, the higher the controllability allowed by a given actuator set, the lower the control energy needed to control the system, i.e. less consumption of fuel or lower risk of saturation for the actuators.

[1] the concept of observability is dual with respect to it but here it is not addressed

There are a lot of studies in this field[13], different concepts are used to define the degree of controllability, where Recovery Region and Balanced Realization are two of the most important ones. Skipping the mathematical derivation which can be found in the quoted text, a fundamental function proposed by Hamdan and Nayfeh and formalized by Junkins and Kim in their book allows to compute each mode's gross measure of controllability once the system matrices A and B are assigned, it will be the first important instrument

$$[\boldsymbol{gMC}] = \mathrm{moc}\,(A, B) \quad \text{where } A, B \in \Re^{n\times n}\ \boldsymbol{gMC} \in \Re^{n}$$

Besides the measure of controllability there is another relevant aspect, it can be named 'modal importance'. A quadratic performance index representing a particular measure of system behavior (i.e. a state error, a displacement of a particular node, etc.) is adopted as the cost function and the actuator input cost analysis can be performed. Basically it concerns the decomposition of the total cost into contribution from each input (actuator), so that the actuator with the largest cost contributes more to the system performance. This concept is really useful when applied in actuator placement optimization, in fact deleting actuators with lowest influence the best configuration can be achieved. This logic can be applied also on the state vector components, leading to the 'component cost analysis', it gives the contribution of each component to the overall performance index. When modal coordinates are chosen it can be useful in model order reduction.

The component cost is defined as the ratio between the cost of the component and the total cost, i.e. the following relation must be verified

$$V = \sum_{i=1}^{n} V_i$$

where n is the number of the components. The total cost function, named also 'objective function' or 'target function', is defined by means of the scalar function

$$\int_0^\infty \boldsymbol{y}^T(t)\, Q \boldsymbol{y}(t)\, dt$$

to give

$$V = \sum_{i=1}^{m} \int_0^\infty {\boldsymbol{y}_d^i}^T(t)\, Q_v \boldsymbol{y}_d^i(t)\, dt \tag{6.1}$$

$$\boldsymbol{y}_d^i(t) = C_d \boldsymbol{x}^i(t)$$

where Q_v (usually taken as a diagonal matrix) is a weighting matrix and C_d is defined so that $\boldsymbol{y}_d$ models and important output for the design objectives.

The mathematics needed to compute the modal cost is not straightforward and here it is omitted for the sake of simplicity, it can be found in the referenced text. As a final remark it should be noticed that when modal coordinates are used and the component cost analysis is applied on the state vector, the output gives directly the relative cost of each mode of the system, i.e. the system modal cost.

6.1.1 Modal Cost for Second Order Systems

When dealing with vibrating mechanical systems, it is usual to encounter systems of n second–order differential equations in the form

$$M\ddot{\boldsymbol{x}} + C\dot{\boldsymbol{x}} + K\boldsymbol{x} = D\boldsymbol{u}$$

with $\boldsymbol{x} \in \Re^n$ and $\boldsymbol{u} \in \Re^m$ are state and control vectors respectively, M is an $n \times n$ positive definite symmetric mass matrix, C is an $n \times n$ positive semidefinite symmetric structural damping matrix, K is an $n \times n$ positive semidefinite stiffness matrix and D is an $n \times m$ control influence matrix.

If modal coordinates are used three major benefits arise:

- simplified computational processes due to the uncoupling of the equations;
- each state's contribution to the cost function corresponds to the modal cost;
- the inherent 'frequency ordering' is of invaluable importance in order reduction processes.

The modal coordinate transformation can be stated as follows

$$\boldsymbol{x}(t) = \Phi\boldsymbol{\eta}(t)$$

where Φ is the modal matrix obtained by solving the eigenvalue problem (its columns are the related eigenvectors) associated with the nominal mass and stiffness matrices, and $\eta(t)$ is the $n \times 1$ modal coordinates vector. The equation of motion in terms of modal coordinates becomes

$$\tilde{M}\ddot{\boldsymbol{\eta}} + \tilde{C}\dot{\boldsymbol{\eta}} + \tilde{K}\boldsymbol{\eta} = \tilde{D}\boldsymbol{u}$$

where the transformed matrices are

$$\begin{aligned}
\tilde{M} &= \Phi^T M \Phi = I \\
\tilde{C} &= \Phi^T C \Phi = \mathrm{diag}\left(2\zeta_1\omega_1, ..., 2\zeta_n\omega_n\right) \\
\tilde{K} &= \Phi^T K \Phi = \mathrm{diag}\left(\omega_1^2, ..., \omega_n^2\right) \\
\tilde{D} &= \Phi^T D
\end{aligned}$$

In this case the diagonal shape of matrix C requires it to be a linear combination of mass and stiffness matrices (i.e. modal damping).

Especially when dealing with FEM models generated matrices, their order can be really large. In such cases model reduction is almost always an unavoidable process. There are a lot of different ways to perform a model order reduction, some of them are[38]

- minimal transfer equivalent realizations;
- matching frequencies and power moments;
- balanced realization;
- truncation;
- singular perturbation.

In what follows just one of them will be applied, the truncation method. When the prescribed order is defined (i.e. order $n_{sys} = 10$ or $n_{sys} = 20$), it basically consists in transforming the system from physical to modal coordinates and then cropping all the matrices (and by consequence related state vectors) to their upper–left square part of $n_{sys} \times n_{sys}$ dimensions, while in case of the control influence matrix it will be cropped to its upper rectangular part of $n_{sys} \times m$ dimensions.

System dynamics is usually described by means of first–order differential system, it is possible to rewrite the starting equation by means of the following $2n \times 1$ modal state vector

$$\boldsymbol{z} = \left\{ \begin{array}{c} \boldsymbol{\eta} \\ \\ \dot{\boldsymbol{\eta}} \end{array} \right\}$$

so that the system becomes

$$\dot{\boldsymbol{z}} = A\boldsymbol{z} + B\boldsymbol{u}$$

where

$$A = \left[\begin{array}{cc} 0 & I \\ \\ -\tilde{K} & -\tilde{C} \end{array} \right], \quad B = \left[\begin{array}{c} 0 \\ \\ \tilde{D} \end{array} \right]$$

The system performance measure to evaluate the cost function is usually chosen as in equation 6.1 with

$$\boldsymbol{y}_d\,(t) = \left[\begin{array}{cc} C_{dx} & 0 \\ \\ 0 & C_{d\dot{x}} \end{array} \right] \left\{ \begin{array}{c} \boldsymbol{x}\,(t) \\ \\ \dot{\boldsymbol{x}}\,(t) \end{array} \right\} \equiv Cd \left\{ \begin{array}{c} \boldsymbol{x}\,(t) \\ \\ \dot{\boldsymbol{x}}\,(t) \end{array} \right\}$$

and with the suitable choice of C_d this quantity becomes a vector of physically important variable. Then the output weighting matrix has to be chosen, the following structure can be adopted

$$Q_v = \begin{bmatrix} Q_x & 0 \\ 0 & Q_{\dot{x}} \end{bmatrix}$$

When the modal transformation is introduced the output vector can be related to modal coordinates as follows.

$$\boldsymbol{y}_d(t) = C_d \begin{Bmatrix} \Phi\boldsymbol{\eta}(t) \\ \Phi\dot{\boldsymbol{\eta}}(t) \end{Bmatrix} = \begin{bmatrix} C_{dx}\Phi & 0 \\ 0 & C_{d\dot{x}}\Phi \end{bmatrix} \begin{Bmatrix} \boldsymbol{\eta}(t) \\ \dot{\boldsymbol{\eta}}(t) \end{Bmatrix} \equiv C_{d\eta} \begin{Bmatrix} \boldsymbol{\eta}(t) \\ \dot{\boldsymbol{\eta}}(t) \end{Bmatrix}$$

The modal cost V_i represents the contribution of the $-ith$ mode to the total cost V, thus the normalized modal cost V_i/V provides a measure of each mode's relative contribution to the system performance. Basically it can be resumed with a function like the next one, which will be the second useful instrument

$$[V, V_i] = \text{modcst}\,(M, C, K, D, \Phi, C_x, C_{xd}, Q_x, Q_{xd})$$

with the common meaning of the involved terms.

6.1.2 Controllability for Actuator Placement

When a given actuator set is chosen it is possible to evaluate the gross measure of controllability of each mode and the modal cost by means of the two instruments previously presented (**moc** and **modcst**). It is possible to combine these two quantities in order to define a new measure of controllability. This would take into account not only the gross measure of controllability, but also the relative mode importance for the selected output cost function. It appears so quite natural to define the following quantity which make use of the previously defined quantities

$$\alpha = \sum_{i=1}^{n} \frac{V_i}{V} \rho_i^2$$

where α will be named weighted controllability index and it will be used as the performance index in the actuator placement optimization problem.

It has been said that the more controllable the system, the less critical should generally be the controller. In order to highlight so, it is possible to

evaluate a simple standard state feedback control law and to compare the trend of the α index with the trend of the controller gain, that gives a rough idea of the criticality of the controller, for different sets of actuators. These variables should be negatively correlated, i.e. when α grows the gain should decrease.

For the control law a Linear Quadratic Regulator can be chosen, it derives the required state feedback gain vector minimizing the energy of the states and controls, i.e. the performance index is

$$J = \int_0^\infty \left(\boldsymbol{z}^T Q \boldsymbol{z} + \boldsymbol{u}^T R \boldsymbol{u} \right) dt$$

where

$$\boldsymbol{z} = \begin{pmatrix} \boldsymbol{\eta} \\ \dot{\boldsymbol{\eta}} \end{pmatrix}, \quad Q = \begin{bmatrix} \Omega & 0 \\ 0 & I \end{bmatrix}, \quad R = kI$$

if the gain norm is taken it can be simply employed as indication of criticality of the controller.

Optimal Actuators Location Algorithm

The search for optimal actuator locations can be performed by means of different methods. In case the problem is treated as continuous common gradient based methods can be used, but usually available actuator spots in the structure are discretely distributed. In case the number of them is very large it can lead to very computational demanding algorithms. Skelton proposed an heuristic algorithm which is reported in [13], that is briefly recalled hereafter. The problem consist to find a number n_{act} of actuators with N available spots. All the available spots are initially fulfilled with actuators. Then the performance index α is evaluated for each of the N combinations obtained removing one actuator at a time. The best combination (with the highest α value) of $N-1$ actuators is chosen and the process is iterated until the number of active actuators reaches the prescribed n_{act}. In steps it is

1. Initialize the starting configuration of N actuators
2. Calculate the α index for each of the N combinations obtained removing each actuator one at a time
3. Select the best configuration from step 2
4. Iterate step 2 and 3 until the prescribed actuator number n_{act}

It should be noticed that this algorithm causes a number of performance index evaluations N_{eval}

$$N_{eval} = \sum_{i=n_{act}}^{N} i$$

which in case of about 200 available spots and a prescribed actuators number of 3 means about 20000 performance index evaluations.

6.2 Case Study

In this section all concepts recalled in last three chapters are applied in a case study. A flexible structure is considered: the FEM model developed in Chapter 4 is applied, so that the system matrices K, C and M are known. The problem can be seen as a second–order mechanic system dynamical analysis. Given the FEM model it is possible to directly apply the concepts described in this chapter in order to obtain a measure of the system controllability, mixing the two instruments **moc** and **modcst**. This quantity, α, is the cost function to be maximized. This task is performed by means of the heuristic algorithm proposed by Junkins and Kim (Skelton's algorithm - SKE) and then by means of some stochastic algorithms that have been described in the dedicated Chapter. In particular three of them have been used and compared: Particle Swarm Optimization - PSO, Genetic Algorithm - GA and Differential Evolution - DE. Results are presented in terms of algorithms output and computational time. Stochastic algorithms have been run 20 times for each configuration, in order to evaluate statistically how often do they reach the optimum.

6.2.1 Model

All model inputs are presented in the code listed here. The structure is supposed to be a two–dimensional beams frame presented in fig. 6.1. The mesh is uniform and each sub–structure has $n_{el} = 5$ beam–like elements. The number of actuators n_{act} has been chosen equal to 3 and only torque actuators have been considered (like reaction wheels or control moment gyros). The structure dimensions have been limited in order to maintain the matrices small enough to easily perform calculations but the natural frequencies match those hypothesized for the SPS concepts[44]. The selected material is classic *Al* 2024. The system order for the model reduction has been chosen equal to 10, as explained in the dedicated section, the system reduction method employed is the truncation method.

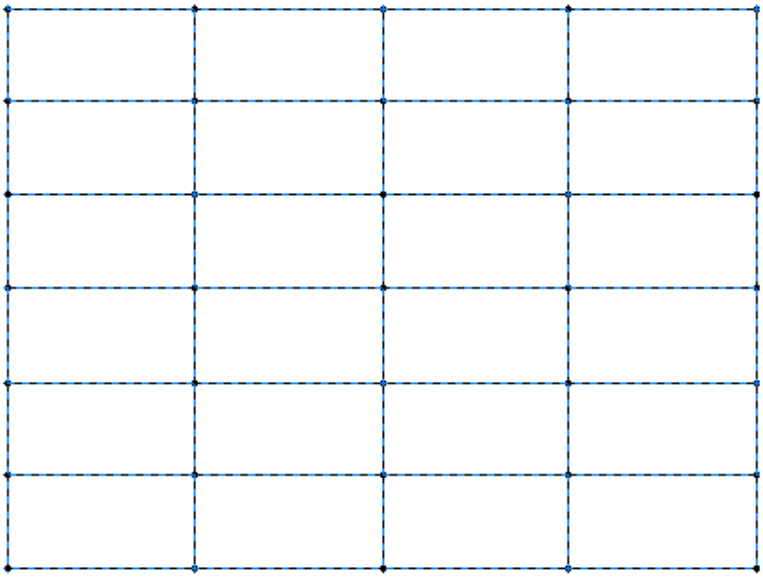

Figure 6.1: Flexible structure geometry

```
Geometry and FEM Mesh

Lx = 5;          % [m] x-edge length
Ly = 5;          % [m] y-edge length
column_num = 6; % number of x-edges
row_num = 6;     % number of y-edges
n_el = 5;          % number of elements edge

act_num = 3;   % number of actuators

% Material Properties
radius = 0.005;               % [m] Section Radius
nu = 0.33;                    % [] Poisson Modulus
par(1) = 73.1e9;              % [N/m^2] Young Modulus
par(2) = par(1)/(2*(1+nu));  % [N/m^2] Shear Modulus
par(3) = pi*radius^2;         % [m^2] Beams Area
par(4) = pi*radius^4/2;       % [m^4] Polar Inertia Moment
par(5) = pi*radius^4/4;       % [m^4] Moment of Inertia y-axis
par(6) = pi*radius^4/4;       % [m^4] Moment of Inertia z-axis
par(7) = 2800;                % [kg/m^3] Density
par(8) = NaN;                 % [] Damping Matrix K Coefficient
```

```
par(9) = NaN;                   % [] Damping Matrix M Coefficient
par(10) = 0.001;                % Damping Global Coefficient

sys_order = 10;
```

With these input values the structure has a total nodes number of $N_{nodes} = 385$ and a number of beam crossing joints of $joint_{num} = 49$. With these choices matrices dimensions are 2310×2310. The first natural frequency is $\sqrt{K_t(1,1)} = 0.0665$ rad/s. It has been chosen to limit the actuator location only in the beam crossing joints. Their numeration, consistent with the global one, is presented here

```
  |  y-axis
  |
 355--360--365--370--375--380--385
  |    |    |    |    |    |    |
 296--301--306--311--316--321--326
  |    |    |    |    |    |    |
 237--242--247--252--257--262--267
  |    |    |    |    |    |    |
 178--183--188--193--198--203--208
  |    |    |    |    |    |    |
 119--124--129--134--139--144--149
  |    |    |    |    |    |    |
  60---65---70---75---80---85---90
  |    |    |    |    |    |    |
   1----6---11---16---21---26---31---> x-axis
```

Optimization outputs will be referred to this numeration to indicate where the actuators are located.

6.2.2 Output Function

As seen previously in this chapter, in order to study the actuator placement optimization, it is needed to define an output function that is of particular design interest. In this case two different outputs functions have been used:

- the first one minimizes the displacement of the entire lower edge (x–axis);
- the second one minimizes the excitation of the first mode of the structure (1^{st} mode).

α	Actuators	Orientation
0.0041186	[178, 208, 370]	[y, y, x]

Table 6.1: Skelton algorithm result, target function x–axis

The reasons for the first choice is directly linked to the possibility of mounting a particular equipment on the selected edge, the result can be generalized since the structure is symmetric. While the second choice is justified by the fact that the first mode is the one with the lower natural frequency so that the first to be exited by external disturbances.

6.2.3 Optimization Results

Here all the optimization results are presented. The Skelton algorithm results will be taken as a reference, with respect to them the stochastic algorithms are compared.

The number of parameters to be optimized is directly dependent on the number of actuators. Each actuator is, in fact, identified by two numbers: the first one is the node number where the actuator will be located (in the treated case this number will be chosen from the joint nodes), and the second number identifies the direction of the actuator x, y o z (i.e. the direction of the torque applied by the actuator). So in the considered case the parameters number is $N_p = n_{act} \cdot 2 = 6$.

Skelton Algorithm - SKE

The output of Skelton algorithm shows which is the best configuration that maximizes the system controllability for the two output functions. In both cases the best solution has the three actuators located at the center of each edge but the x–axis and directed along the edge itself, see table 6.1 and 6.2. It has to be underlined that basically the problem has four optimal solutions with the same value of controllability, these solutions are represented by the combination of the three actuators in three of the four edges center. As it will be shown in what follows, sometimes the stochastic algorithm finds one of the other three solutions instead of the one presented here, but it can be considered the global optimum.

α	Actuators	Orientation
0.0035762	[178, 208, 370]	[y, y, x]

Table 6.2: Skelton algorithm result, target function 1^{st} mode

Particle Swarm Optimization - PSO

The following list resumes the PSO algorithm options used for this problem. First four parameters define that the algorithms stops if a maximum iteration number is reached or if the performance index does not improve of a certain amount for a given number of iterations. Last three parameters are the coefficients that rule the movement of the individuals inside the domain of search (see dedicated section).

```
PSO Options (Number of individuals = 5*Np)
pso(1) = 2;     % Stop Test(1-Max Iter Number, 2-Min d(P.I.))
pso(2) = 0.001; % Mininum d(P.I.) w.r.t. Maximum P.I. Value
pso(3) = 15;    % Maximum Number of times d(P.I.)<min
pso(4) = 300;   % Maximum Iterations
pso(5) = 2;     % c1 defalut = 2
pso(6) = 2;     % c2 defalut = 2
pso(7) = 0.3;   % c3 intertia
```

Two tables are presented, the first one, table 6.3, is referred to the first case (x-axis output function) while the second one, table 6.4, present data for the first mode controllability. It can be seen that the success rate is of $11/20 = 55\%$ and $13/20 = 65\%$ respectively.

Run	α	Actuators	Orientation
1	0.0041186	[178, 208, 370]	[y, y, x]
2	0.0041186	[178, 208, 370]	[y, y, x]
3	0.0041186	[178, 208, 370]	[y, y, x]
4	0.0041186	[178, 208, 370]	[y, y, x]
5	0.0041186	[178, 208, 370]	[y, y, x]
6	0.0041186	[178, 208, 370]	[y, y, x]
7	0.0041186	[178, 208, 370]	[y, y, x]
8	0.0041186	[178, 208, 370]	[y, y, x]
9	0.0041112	[16, 208, 370]	[x, y, x]
10	0.0041112	[16, 208, 370]	[x, y, x]
11	0.0041112	[16, 208, 370]	[x, y, x]
12	0.0039291	[208, 365, 370]	[y, x, x]
13	0.0039291	[208, 365, 370]	[y, x, x]
14	0.0039291	[208, 365, 370]	[y, x, x]
15	0.0039291	[208, 365, 370]	[y, x, x]
16	0.0039230	[16, 365, 370]	[x, x, x]
17	0.0039230	[16, 365, 370]	[x, x, x]
18	0.0039229	[16, 21, 370]	[x, x, x]
19	0.0039229	[16, 21, 370]	[x, x, x]
20	0.0039229	[16, 21, 370]	[x, x, x]

Table 6.3: PSO algorithm result, target function x–axis

Run	α	Actuators	Orientation
1	0.0035762	[178, 208, 370]	[x, x, y]
2	0.0035762	[178, 208, 370]	[x, x, y]
3	0.0035762	[178, 208, 370]	[x, x, y]
4	0.0035762	[178, 208, 370]	[x, x, y]
5	0.0035762	[178, 208, 370]	[x, x, y]
6	0.0035762	[178, 208, 370]	[x, x, y]
7	0.0035762	[16, 208, 370]	[y, x, y]
8	0.0035762	[16, 208, 370]	[y, x, y]
9	0.0035762	[16, 208, 370]	[y, x, y]
10	0.0035762	[16, 208, 370]	[y, x, y]
11	0.0035762	[16, 208, 370]	[y, x, y]
12	0.0035762	[16, 208, 370]	[y, x, y]
13	0.0035762	[16, 208, 370]	[y, x, y]
14	0.0034372	[178, 208, 267]	[x, x, x]
15	0.0034372	[16, 21, 208]	[y, y, x]
16	0.0034372	[16, 21, 208]	[y, y, x]
17	0.0034372	[16, 21, 208]	[y, y, x]
18	0.0034372	[16, 21, 370]	[y, y, y]
19	0.0034372	[16, 21, 370]	[y, y, y]
20	0.0029062	[1, 178, 370]	[x, x, y]

Table 6.4: PSO algorithm result, target function 1^{st} mode

Genetic Algorithm - GA

The following list resumes the GA algorithm options used for this problem. First four parameters define that the algorithms stops if a maximum iteration number is reached or if the performance index does not improve of a certain amount for a given number of iterations. The fifth parameter represent the choice of the reproduction method. Last five parameters are the coefficients that rule the natural selection patterns and events (see dedicated section).

```
GA Options (Number of individuals = 10*Np)
ga(1)  = 2;     % Stop Test(1-Max Iter Number, 2-Min d(P.I.))
ga(2)  = 0.001; % Mininum d(P.I.) w.r.t. Maximum P.I. Value
ga(3)  = 15;    % Maximum Number of times d(P.I.)<min
ga(4)  = 300;   % Maximum Iterations
ga(5)  = 2;     % ga_method: 1-Double Point, 2-Heuristic
ga(6)  = 0.1;   % Elitism Percentual [0-1] of total population
ga(7)  = 1.2;   % R (Heuristic) default value = 1.2
ga(8)  = 0.05;  % Mass Extinction Survivor total population %
ga(9)  = 10;    % Mass Extinction Flag, n° of times d(P.I.)<min
ga(10) = 2;     % Max Number of Mass Extinctions
```

Two different reproduction methods will be used with both output functions, so that four tables will be presented.
Double Crossover. Table 6.5 is referred to the first output function (x–axis) while table 6.6 presents data for the first mode controllability, both in case of double crossover reproduction method. It can be seen that the success rate is of $6/20 = 30\%$ and $5/20 = 25\%$ respectively.
Weighted Average. Table 6.7 is referred to the first output function (x–axis) while table 6.8 presents data for the first mode controllability, both in case of weighted average reproduction method. It can be seen that the success rate is of $5/20 = 25\%$ and $4/20 = 20\%$ respectively.

Run	α	Actuators	Orientation
1	0.0041186	[178, 208, 370]	[y, y, x]
2	0.0041186	[178, 208, 370]	[y, y, x]
3	0.0041186	[178, 208, 370]	[y, y, x]
4	0.0041112	[16, 208, 370]	[x, y, x]
5	0.0041112	[16, 208, 370]	[x, y, x]
6	0.0041112	[16, 208, 370]	[x, y, x]
7	0.0039229	[16, 242, 355]	[y, x, x]
8	0.0039109	[11, 203, 360]	[y, x, z]
9	0.0037610	[11, 16, 139]	[y, x, x]
10	0.0036813	[80, 129, 188]	[x, x, y]
11	0.0036766	[11, 16, 188]	[z, z, x]
12	0.0036766	[1, 183, 237]	[z, y, z]
13	0.0036090	[134, 198, 321]	[x, y, y]
14	0.0035955	[124, 262, 380]	[z, x, z]
15	0.0035251	[65, 262, 380]	[x, z, z]
16	0.0035002	[208, 208, 178]	[x, z, y]
17	0.0034867	[306, 311, 380]	[x, y, z]
18	0.0034620	[124, 242, 296]	[z, x, y]
19	0.0034548	[11, 16, 306]	[y, x, z]
20	0.0034476	[208, 301, 360]	[x, z, z]

Table 6.5: GA (Double Crossover) algorithm result, target function x–axis

Run	α	Actuators	Orientation
1	0.0035762	[178, 208, 370]	[x, x, y]
2	0.0035762	[178, 208, 370]	[x, x, y]
3	0.0035762	[16, 208, 370]	[y, x, y]
4	0.0035762	[16, 208, 370]	[y, x, y]
5	0.0035762	[16, 208, 370]	[y, x, y]
6	0.0034372	[6, 21, 198]	[y, x, z]
7	0.0032982	[26, 119, 296]	[z, y, y]
8	0.0032982	[183, 311, 316]	[z, x, z]
9	0.0032982	[21, 149, 247]	[z, x, z]
10	0.0032982	[16, 242, 321]	[z, y, z]
11	0.0032982	[16, 60, 257]	[x, z, z]
12	0.0031593	[26, 119, 149]	[y, z, x]
13	0.0031593	[183, 193, 380]	[z, y, z]
14	0.0031593	[183, 208, 257]	[z, y, y]
15	0.0031324	[129, 149, 311]	[x, y, x]
16	0.0029934	[90, 257, 262]	[x, x, y]
17	0.0029934	[1, 75, 149]	[x, z, x]
18	0.0029934	[237, 316, 355]	[y, y, y]
19	0.0029934	[21, 242, 301]	[x, y, x]
20	0.0029934	[1, 237, 301]	[z, z, y]

Table 6.6: GA (Double Crossover) algorithm result, target function 1^{st} mode

Run	α	Actuators	Orientation
1	0.0041186	[178, 208, 370]	[y, y, x]
2	0.0041186	[178, 208, 370]	[y, y, x]
3	0.0041112	[16, 208, 370]	[x, y, x]
4	0.0041112	[16, 208, 370]	[x, y, x]
5	0.0041112	[16, 208, 370]	[x, y, x]
6	0.0039229	[6, 6, 306]	[x, y, y]
7	0.0039229	[6, 6, 306]	[x, y, y]
8	0.0039229	[6, 6, 306]	[x, y, y]
9	0.0037659	[11, 80, 267]	[y, y, z]
10	0.0037659	[11, 80, 267]	[y, y, z]
11	0.0037659	[11, 80, 267]	[y, y, z]
12	0.0036524	[252, 316, 365]	[z, x, y]
13	0.0036524	[252, 316, 365]	[z, x, y]
14	0.0036524	[252, 316, 365]	[z, x, y]
15	0.0036524	[252, 316, 365]	[z, x, y]
16	0.0036524	[252, 316, 365]	[z, x, y]
17	0.0036090	[188, 262, 360]	[y, x, x]
18	0.0036090	[188, 262, 360]	[y, x, x]
19	0.0036090	[188, 262, 360]	[y, x, x]
20	0.0036090	[188, 262, 360]	[y, x, x]

Table 6.7: GA (Weighted Parents Average) algorithm result, target function x–axis

Run	α	Actuators	Orientation
1	0.0035762	[178, 208, 370]	[x, x, y]
2	0.0035762	[178, 208, 370]	[x, x, y]
3	0.0035762	[178, 208, 370]	[x, x, y]
4	0.0035762	[16, 208, 370]	[y, x, y]
5	0.0034372	[124, 188, 321]	[z, z, x]
6	0.0034372	[124, 188, 321]	[z, z, x]
7	0.0034372	[124, 188, 321]	[z, z, x]
8	0.0031593	[21, 296, 360]	[y, z, y]
9	0.0031593	[21, 296, 360]	[y, z, y]
10	0.0031593	[21, 296, 360]	[y, z, y]
11	0.0031324	[198, 262, 321]	[x, z, z]
12	0.0031324	[198, 262, 321]	[x, z, z]
13	0.0031324	[198, 262, 321]	[x, z, z]
14	0.0029368	[134, 296, 301]	[x, y, x]
15	0.0029368	[134, 296, 301]	[x, y, x]
16	0.0029368	[134, 296, 301]	[x, y, x]
17	0.0029062	[80, 203, 247]	[y, z, x]
18	0.0029062	[80, 203, 247]	[y, z, x]
19	0.0029062	[80, 203, 247]	[y, z, x]
20	0.0029062	[80, 203, 247]	[y, z, x]

Table 6.8: GA (Weighted Parents Average) algorithm result, target function 1^{st} mode

Differential Evolution - DE

The following list resumes the DE algorithm options used for this problem. First four parameters define that the algorithms stops if a maximum iteration number is reached or if the performance index does not improve of a certain amount for a given number of iterations. The fifth parameter represent the choice of the new individuals creation. Last three parameters are the coefficients that rule the chosen individual creation method (see dedicated section).

```
DE Options (Number of individuals = 5*Np)
de(1) = 2;     % Stop Test(1-Max Iter Number, 2-Min d(P.I.))
de(2) = 0.001; % Mininum d(P.I.) w.r.t. Maximum P.I. Value
de(3) = 15;    % Maximum Number of times d(P.I.)<min
de(4) = 300;   % Maximum Iterations
de(5) = 1;     % de_method(1-best 2-rand)
de(6) = 0.7;   % F [0.5 - 0.9]
de(7) = 0.7;   % C [0.5 - 0.9]
de(8) = 0.9;   % CR [0.8 - 0.9]
```

Two different reproduction methods will be used with both output functions, so that four tables will be presented.
x_1 **best**. Table 6.9 is referred to the first output function (x–axis) while table 6.10 presents data for the first mode controllability, both in case of new generations created starting from x_1 = best individual. It can be seen that the success rate is of $8/20 = 40\%$ and $7/20 = 35\%$ respectively.
x_1 **random**. Table 6.11 is referred to the first output function (x–axis) while table 6.12 presents data for the first mode controllability, both in case of new generations created starting from x_1 = random individual. It can be seen that the success rate is of $8/20 = 40\%$ and $7/20 = 35\%$ respectively.

Run	α	Actuators	Orientation
1	0.0041186	[178, 208, 370]	[y, y, x]
2	0.0041186	[178, 208, 370]	[y, y, x]
3	0.0041186	[178, 208, 370]	[y, y, x]
4	0.0041186	[178, 208, 370]	[y, y, x]
5	0.0041186	[178, 208, 370]	[y, y, x]
6	0.0041112	[16, 208, 370]	[x, y, x]
7	0.0041112	[16, 208, 370]	[x, y, x]
8	0.0041112	[16, 208, 370]	[x, y, x]
9	0.0039230	[16, 365, 370]	[x, x, x]
10	0.0039230	[16, 365, 370]	[x, x, x]
11	0.0039230	[16, 365, 370]	[x, x, x]
12	0.0039046	[16, 370, 375]	[x, x, x]
13	0.0037411	[16, 365, 119]	[x, x, y]
14	0.0037411	[16, 365, 119]	[x, x, y]
15	0.0037411	[16, 365, 119]	[x, x, y]
16	0.0037411	[16, 365, 119]	[x, x, y]
17	0.0033192	[149, 178, 385]	[y, y, x]
18	0.0033192	[149, 178, 385]	[y, y, x]
19	0.0033192	[149, 178, 385]	[y, y, x]
20	0.0033192	[149, 178, 385]	[y, y, x]

Table 6.9: DE (x_1 best) algorithm result, target function x–axis

Run	α	Actuators	Orientation
1	0.0035762	[178, 208, 370]	[x, x, y]
2	0.0035762	[178, 208, 370]	[x, x, y]
3	0.0035762	[178, 208, 370]	[x, x, y]
4	0.0035762	[16, 208, 370]	[y, x, y]
5	0.0035762	[16, 208, 370]	[y, x, y]
6	0.0035762	[16, 208, 370]	[y, x, y]
7	0.0035762	[16, 208, 370]	[y, x, y]
8	0.0032982	[119, 178, 237]	[x, x, x]
9	0.0032982	[119, 178, 237]	[x, x, x]
10	0.0032982	[119, 178, 237]	[x, x, x]
11	0.0032982	[119, 178, 237]	[x, x, x]
12	0.0032982	[119, 178, 237]	[x, x, x]
13	0.0032982	[119, 178, 237]	[x, x, x]
14	0.0030060	[178 183, 208]	[x, x, x]
15	0.0030060	[178, 183, 208]	[x, x, x]
16	0.0030060	[178, 183, 208]	[x, x, x]
17	0.0030060	[178, 183, 208]	[x, x, x]
18	0.0029934	[149, 178, 326]	[x, x, x]
19	0.0029934	[149, 178, 326]	[x, x, x]
20	0.0029934	[149, 178, 326]	[x, x, x]

Table 6.10: DE (x_1 best) algorithm result, target function 1^{st} mode

Run	α	Actuators	Orientation
1	0.0041186	[178, 208, 370]	[y, y, x]
2	0.0041186	[178, 208, 370]	[y, y, x]
3	0.0041186	[178, 208, 370]	[y, y, x]
4	0.0041186	[178, 208, 370]	[y, y, x]
5	0.0041186	[178, 208, 370]	[y, y, x]
6	0.0041112	[16, 208, 370]	[x, y, x]
7	0.0041112	[16, 208, 370]	[x, y, x]
8	0.0041112	[16, 208, 370]	[x, y, x]
9	0.0037606	[11, 16, 365]	[x, x, x]
10	0.0037606	[11, 16, 365]	[x, x, x]
11	0.0037606	[11, 16, 365]	[x, x, x]
12	0.0037606	[11, 16, 365]	[x, x, x]
13	0.0034258	[70, 149, 178]	[x, y, y]
14	0.0034258	[70, 149, 178]	[x, y, y]
15	0.0034258	[70, 149, 178]	[x, y, y]
16	0.0034258	[70, 149, 178]	[x, y, y]
17	0.0032847	[119, 242, 267]	[y, y, y]
18	0.0032847	[119, 242, 267]	[y, y, y]
19	0.0032847	[119, 242, 267]	[y, y, y]
20	0.0032847	[119, 242, 267]	[y, y, y]

Table 6.11: DE (x_1 random) algorithm result, target function x–axis

Run	α	Actuators	Orientation
1	0.0035762	[178, 208, 370]	[x, x, y]
2	0.0035762	[178, 208, 370]	[x, x, y]
3	0.0035762	[178, 208, 370]	[x, x, y]
4	0.0035762	[16, 208, 370]	[y, x, y]
5	0.0035762	[16, 208, 370]	[y, x, y]
6	0.0035762	[16, 208, 370]	[y, x, y]
7	0.0035762	[16, 208, 370]	[y, x, y]
8	0.0029368	[203, 301, 355]	[y, y, y]
9	0.0029368	[203, 301, 355]	[y, y, y]
10	0.0029368	[203, 301, 355]	[y, y, y]
11	0.0029368	[203, 301, 355]	[y, y, y]
12	0.0029368	[203, 301, 355]	[y, y, y]
13	0.0028544	[6, 139, 262]	[y, y, y]
14	0.0028544	[6, 139, 262]	[y, y, y]
15	0.0028544	[6, 139, 262]	[y, y, y]
16	0.0028544	[6, 139, 262]	[y, y, y]
17	0.0023841	[26, 75, 365]	[y, x, z]
18	0.0023841	[26, 75, 365]	[y, x, z]
19	0.0023841	[26, 75, 365]	[y, x, z]
20	0.0023841	[26, 75, 365]	[y, x, z]

Table 6.12: DE (x_1 random) algorithm result, target function 1^{st} mode

Computational time comparison and α index–LQR controller gain relation

In this paragraph different algorithms are compared in terms of computational time and a the relation controllability index α - LQR controller gain is investigated.

It has been said that for SKE algorithm the number of cost function evaluations is obtained by the formula

$$N_{eval} = \sum_{i=n_{act}}^{N} i$$

that in the considered case, where $N = 3 \cdot joint_{num} = 3 \cdot 49 = 147$ and $n_{act} = 3$, gives $N_{eval} = 10875$. For the stochastic algorithms the number of performance index evaluations is easily calculable, it is given simply by the dot product of the number of individuals present inside the optimizer multiplied by the iterations number. This number can be considered directly proportional to the algorithms computational time, even if it is an approximation since each algorithm after the performance index evaluation performs its own calculation. For this reason it is useful also to directly evaluate the time for for each algorithm with same initial conditions. In table 6.13 both quantities are reported: it is quite evident how the stochastic optimizers are definitely faster both in terms of computational time and number of performance index evaluations. It is clear that the stochastic optimizer does not provide the certainty to find the optimum on each run, but it is also true that in case of very large matrices the use of stochastic algorithms could be a very useful instruments in order to have preliminary informations in a fast way, while Skelton Algorithm may become not feasible.

Another important aspect is that it appears that to change the reproduction/generation method does not affect significantly the algorithm performance in terms of success rate for this problem, it happened both in case of DE and GA. For the GA, that is however the worse algorithm, also a change in the elitism and mass extinction parameters did not improve the success rate.

From the present discussion and previous data the best choice would be the PSO optimizer, it combines accuracy/successful rate in the optimum search with the best speed of convergence. The worse one is for sure the GA optimizer which is quite inaccurate and the slowest one among the three of them.

In figure 6.2 the relation between the structure controllability index α and the LQR gain norm evaluated for the corresponding actuator configuration

	SKE	PSO	GA	DE
CPU Time [sec]	1059.8061	13.3620	53.1801	15.5745
Iterations [ ]	-	32	43	33
P.I. Evaluations [ ]	10875	160	215	165
Success Rate [%]	100	55-65	20-30	35-40

Table 6.13: Performances comparison

is presented. The two quantities appears to be negatively correlated with a correlation factor of $c = -0.5274$, even if it is not very high it is possible to consider, in a preliminary analysis, α as a good indicator of the global structure controllability.

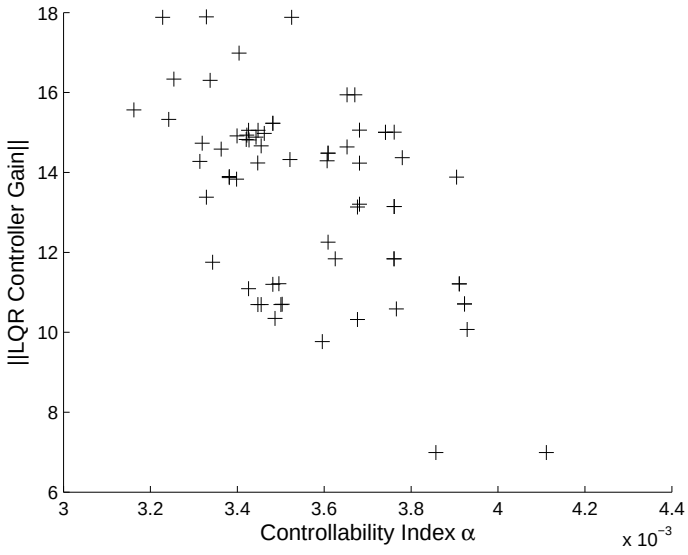

Figure 6.2: α-LQR gain relation. $c = -0.5274$

This page intentionally left blank

Chapter 7

Conclusions and Future Work

7.1 Conclusions

One SPS concept among the total produced by the scientific community has been chosen and two relevant features have been studied. The selected concept, the JAXA reference model 2003, is the first proposed SPS that uses a formation flying configuration. Its dimensions, like other concepts, are huge: collectors and array are about 10 and 2 square kilometers respectively. This feature is responsible for two issues. The first one is generated by solar radiation hitting large surfaces, it would cause orbital and attitude perturbations which cannot be neglected in order to satisfy tight pointing accuracy. The other one is related to the structure flexibility, with dimensions like these it is completely useless and misleading to consider the satellite as a rigid body. First natural frequencies are so low that is practically certain they will be exited during operations. So that, there is the need to build an appropriate flexible structure model both for the attitude control or the actuator placement problem. These two aspects have been treated in this work, exploring new ways to solve perturbed relative orbit in formation flying satellites and actuator placement optimization.

7.1.1 Formation Flying

Among different modern approaches in the formation flying field one proposed by H. Schaub was found particularly interesting. It allows to simply compute relative orbit propagation of two satellites knowing their orbital element difference at initial time and using true anomaly ν as independent variable. This analytically approximated formulation can be adopted when no perturbations act on satellites, in such a case numerical integration has to be performed. Given the features of this formulation it is really suitable

to be merged with the standard perturbation approach, developed in a previous work[28] and recalled in Chapter 2. In fact it provides the first–order approximated analytical orbital parameters variation when a perturbation identified by magnitude ε, azimuth α and elevation β, acts on the satellite.

What came out from this idea is a very interesting approach that allows to propagate formation flying satellites relative orbit even in presence of a perturbation. It needs to solve the Kepler problem for the deputy satellite, thus the time equation has a very important role. Two versions of this equation have been developed, one rigorously first–order accurate, but with some integrals that need numerical evaluation, and the other one slightly less accurate but completely analytical. Both of them were applied for the computation.

As it has been shown in Chapter 3 results prove that there is not a big difference in terms of error between the analytical (less accurate) form and the rigorous first–order one, while it is clear that in terms of computational time the analytical relation outperforms the other one. The error with respect to the numerical accurate propagation is below 3% for one entire propagated orbit (x and z components error is below 1%).

The possibility to have an instrument able to propagate formation flying relative orbit in case of perturbed flight is of major importance, it can take into account all disturbances generated by solar radiation or atmosphere drag but it can also be capable of simulate motion under a low thrust propulsion like electric thrusters or solar sails. This latter aspect is fundamental in case of the selected concept since it will fly with two reflectors in a non–Keplerian (i.e. continuously propelled) GEO orbit. The analytical method appears to be really useful in preliminary study phases since it is about 1500 times faster than the numerical one while it maintains a good accuracy.

7.1.2 Actuator Placement

In order to address the problem of actuator placement for flexible structures the first step is to build a model of the structure. Infinite dimensional model are impossible to be developed for complex systems, so that finite dimensional models need to be built. One of the most common ways to do so is to use Finite Element Models. FEM theory has been recalled in Chapter 4 and it is then used to build a two–dimensional model of the SPS array panel. Concepts of controllability and modal cost for dynamical systems have been recalled and a global system controllability α index is built. This parameter depends on where the actuators are located in the structure and the higher its value the more the system can be successfully controlled. This latter aspect of the system can be evaluated in a simplified way evaluating the

LQR feedback controller gain norm, the higher this value, the lower is the system controllabillity. The α-gain negative correlation has been verified, so that α can be used as cost function in an optimization (maximization) problem. Basic concepts on optimization are recalled in Chapter 5. Some algorithms are present in literature, one of them (Skelton algorithm) is taken as a reference, and three different evolutionary algorithms are applied to the problem: Genetic Algorithm, Differential Evolution and Particle Swarm Optimization. Reults in Chapter 6 show that the three stochastic optimizers have different performances. In particular they are all definitely faster than Skelton algorithm, in particular between 20 and 80 times faster, both in terms of computational time and performance index evaluations. On the other hand their performance in terms of success rate is quite different, in percentage it ranges from about 25% of the Genetic Algorithm to over 60% of the Particle Swarm Optimization method. It is clear that when a stochastic algorithm is run there is no certainty to find the optimum but it is also true that in case of very detailed system models (i.e. large mass and sitffness matrices if FEM modeled) Skelton algorithm may become unfeasible.

Actuator placement optimization can be really important, even in the preliminary phase, in order to define the system layout. To have a flexible instrument able to compute (with a high success rate) the optimal actuator configuration is a major achievement since it conjugates the possibility to perform a great number of analysis in a short time (useful in preliminary design) with the capability to deal with detailed (computational demanding) system model (useful in the last design phase). The PSO algorithm seems to be the perfect candidate for this task since it has a very good success rate and the lowest computational time on a single run.

7.2 Future Work

In this section some possible research topics related with the present work are described. They are divided in two groups, the first one analyze the integration in the system model of actuators and sensors, while in the second one different methods to build the structure model are discussed.

7.2.1 Actuators and Sensors Dynamics

In the whole coverage one important assumption has been implicitly made: actuators are thought with an instantaneous dynamics. No practical system can have an instantaneous dynamics, there will always be a delay time between input and output of the system, even in electronic devices, when

the time scale is very small. This fact is particularly relevant in all control problems: this delay time can be negliable if the system dynamics is order of magnitude slower than the actuator one (i.e. if it has a characteristic time order of magnitude larger than the typical delay time of the actuator). But there are some cases in which if the actuator dynamics is neglected, the whole set of results could become meaningless. In particular in case of structure vibration suppression, neglecting the actuator delay time can cause the opposite effect, i.e. it can excite vibrations depending on the phase shift of the actual control given by the actuator with respect to the one evaluated in theory by the controller.

These aspects make clear how important can be to create a good model of the actuators that will be used in the real project. In case of torque actuators, considered in this work, a simple model can be the following one:

$$J\ddot{\theta} + C_v\dot{\theta} = G_M\frac{V_A - k\dot{\theta}}{R} \Rightarrow J\ddot{\theta} + C\dot{\theta} = G_M\frac{V_A}{R} \quad \text{with} \quad C = C_v + \frac{G_M k}{R}$$

it is built considering the equilibrium equation at the actuator axis, where viscous coefficient and counter electromotive force are taken into account (friction constant force can be also added).

If one wants to add the actuator dynamics to the system a number of states equal to the actuator number should be added (i.e. the actuator states) and mass and damping matrix must be updated depending on the actuators location.

When dealing with control problems another aspect needs to be seriously taken into account, that is sensor dynamics. Classical control law are state feedback control law. In order to know these states a sensor has to be placed in appropriate spots (alternatively model based feedback control can be used). In case sensors are used two main problems arise: observability (i.e. the actual possibility to observe the selected state) and a delay time problem analogous to the one of the actuators. In fact also sensors have a delay time, and it can play the same role as the actuators delay, so that it becomes critical when it is of the same order of magnitude of the system dynamics characteristic time.

7.2.2 Modeling and Model Reduction

In this work the structure has been modeled by means of FEM theory. There are a lot of other methods, one of the most diffused is the assumed modes method. It consists in writing the energy of the system in a general form and to substitute in the displacement function (and its derivatives) a linear combination of the first n modes (where n is chosen by the user, it determines

the accuracy and dimension of the model) of the structure (or a similar one). In case of a rectangular structure as the one studied here, one can use as modes in the linear combination the modes of a thin plate with four free edges. Usually natural modes are know analytically for simple domains, so that these functions can be used as a basis. Once they are substituted into the energy equation a set of n conditions is used to determine the n unknowns (each mode coefficient).

Another important aspect for the structure modeling is the system order reduction. As it has been said in the present work the truncation method has been applied, it basically consist in first to transform the coordinate from physical to modal ones by means of the modal matrix. Then it is possible to choose the system order arbitrarily and to perform the order reduction simply by resizing the matrices in the modal coordinate system to the chosen size. This is perhaps the easiest method but there are some other techniques that are more accurate and that can improve the accuracy, most important ones are listed in [38].

This page intentionally left blank

Bibliography

[1] R.R. Bate, D.D. Mueller, e J.E. White, *Fundamentals of Astrodynamics*, Dover Publications Inc., New York, 1971.

[2] R.H. Battin, *Introduction to Mathematics and Methods in Astrodynamics*, AIAA Education Series, Reston (VA), 1999.

[3] A.E. Bryson Jr, Y.C. Ho, *Applied Optimal Control*, Taylor & Francis Group, New York, 1975.

[4] J.W. Cornelisse, *Rocket Propulsion and Spaceflight Dynamics*, Pitman Publishing, London, 1979.

[5] S. D'Amico, O. Montenbruck, "Proximity Operations of Formation-Flying Spacecraft Using an Eccentricity/Inclination Vector Separation", *Journal of Guidance, Control and Dynamics*, Vol. 29, No. 3, pp. 554-563, May-June 2006.

[6] H.F. Feingold, C. Carrington, "Evaluation and Comparison of SPS Concepts", *Acta Astronautica*, Vol. 53, pp. 547-559, 2003.

[7] H.A. Fujii, T. Watanabe, H. Kojima, K. Sekikawa, N. Kobayashi, "Control of Attitude and Vibration of a Tethered Space Solar Power Satellite", *American Institute of Aeronautics and Astronautics - AIAA*, AIAA 2003-5421, 2003.

[8] T. Fujita, S. Sasaki, D. Joudoi, "Overview of Studies on Large Structure for Space Solar Power Systems (SSPS)", *International Astronautical Congress - IAC*, IAC-10-C3.2.9, 2010.

[9] P.E. Glaser, "Satellite Solar Power Station", *Solar Energy*, Vol. 12, pp. 353-361, Pergamon Press, 1969.

[10] P.E. Glaser, "Power From The Sun: Its Future", *Science*, Vol. 162, Number 3856, 1968.

[11] K. Ishimura, K. Higuchi, "Coupling between structural deformation and attitude motion of large planar space structures suspended by multi-tethers", *Acta Astronautica*, Vol. 60, pp. 691-710, 2007.

[12] F. Jiang, J. Li, H. Baoyin, Y. Gao, "Study on Relative Orbit Geometry of Spacecraft Formations in Elliptical Reference Orbits", *Journal of Guidance, Control and Dynamics*, Vol. 31, No. 1, pp. 123-134, January-February 2008.

[13] J.L. Junkins, Y. Kim, *Introduction to Dynamics and Control of Flexible Structures*, AIAA Education Series, Washington DC, 1993.

[14] R. Kristiansen, E.I. Grotli, P.J. Nicklasson, J.T. Gravdahl, "A model of relative translation and rotation in leader-follower spacecraft formations", *Modeling, Identification and Control*, Vol. 28, No. 1, pp. 3-13, 2007.

[15] R. Kristiansen, P.J. Nicklasson, "Spacecraft formation flying: A review and new results on state feedback control", *Acta Astronautica*, Vol. 65, pp. 1537-1552, 2009.

[16] G.A. Landis,"Reinventing the Solar Power Satellite", *International Astrunautical Congress - IAC*, IAC-02-R.3.06, 2004.

[17] G.R. Liu, S.S. Quek, *The Finite Element Method*, Elsevier Science Ltd., Burlington (MA), 2003.

[18] J.C. Mankins, "A Fresh Look at Space Solar Power: New Architectures, Concepts and Technologies", *Acta Astronautica*, Vol. 41, Nos. 4-10, pp. 347-359, 1997.

[19] J.C. Mankins, "A Technical Overview of the 'SunTower' Solar Power Satellite Concept", *Acta Astronautica*, Vol. 50, No. 6, pp. 369-377, 1999.

[20] J.C. Mankins, "New directions for space solar power", *Acta Astronautica*, Vol. 65, pp. 146-156, 2009.

[21] N.I. Marxwell,"An Economic Analysis of Space Solar Power and Its Cost Competitiveness as a Supplemental Source of Energy for Space and Ground Markets", *International Astrunautical Congress - IAC*, IAC-02-R.3.05, 2002.

[22] M. Mori, H. Nagayama, Y. Saito, H. Matsumoto,"Summary of studies on space solar power systems of the National Space Development Agency of Japan", *Acta Astronautica*, Vol. 54, pp. 337-345, 2004.

[23] M. Mori, H. Kagawa, Y. Saito,"Summary of studies on space solar power systems of Japan Aerospace Exploration Agency (JAXA)", *Acta Astronautica*, Vol. 59, pp. 132-138, 2006.

[24] M. Nagatomo, S. Sasaki, Y. Naruo, "Conceptual Study of a Solar Power Satellite, SPS 2000", *Proc. ISTS*, Paper No. ISTS-94-e-04, 1994.

[25] NASA - U.S.A. DOE, *Satellite Power System (SPS) Concept Development and Evaluation Program Plan*, February 1978.

[26] NASA - U.S.A. DOE, *Concept Development and Evaluation Program*, October 1978.

[27] NSSO, "Phase 0 Architecture Feasibility Study", *Space Based Solar Power As an Opportunity for Strategic Security*, October 2007.

[28] A. Palmas, "Approximation of Low Thrust Trajectory Arcs by means of Perturbative Approaches", *M.Sc. Thesis*, Politecnico di Torino, July 2010.

[29] F. Zuiani, M. Vasile, A. Palmas, G. Avanzini "Direct Transcription of Low–Thrust Trajectories with Finite Trajectory Elements", *International Astronautical Congress - IAC*, IAC-10-C1.7.5, 2010.

[30] S.D. Potter, "Alternative Architecture for Commercial SPS", *National Space Society International Space Development Conference*, Tucson - Arizona, May 26-29, 2000.

[31] H.O. Ruppe, "SPS Revisited", *Acta Astronautica*, Vol. 25, No. 10, p. 667, 1991.

[32] S. sasaki, K. Tanaka, K. Higuchi, N. Okuizumi, S. Kawasaki, N. Shinohara, K. Senda, K. Ishimura,"A new concept of solar power satellite: Tethered-SPS", *Acta Astronautica*, Vol. 60, pp. 153-165, 2006.

[33] H. Schaub, K.T. Alfriend, "Hybrid Cartesian and Orbit Element Feedback Law for Formation Flying Spacecraft", *Journal of Guidance, Control and Dynamics*, Vol. 25, No. 2, pp. 387-393, March-April 2002.

[34] H. Schaub, "Relative Orbit Geometry Through Classical Orbit Element Differences", *Journal of Guidance, Control and Dynamics*, Vol. 27, No. 5, pp. 839-848, September-October 2004.

[35] H. Schaub, S.R. Vadali, J.L. Junkins, K.T. Alfriend, "Spacecraft Formation Flying Control using Mean Orbit Elements", *Journal of the Astronautical Sciences*, Vol. 48, No. 1, pp. 69-87, Jan.-March 2000.

[36] W. Seboldt, M. Klimke, M. Leipold, N. Hanowski,"European Sail Tower SPS Concept", *Acta Astronautica*, Vol. 48, Nos. 5-12, pp. 785-792, 2001.

[37] W. Seboldt, "Space and Earth based solar power for the growing energy needs of future generations", *Acta Astronautica*, Vol. 55, pp. 389-399, 2004.

[38] R.E Skelton, M.C. de Oliveira, J.H. Han "System modeling and model reduction", *Internal Report - MAE, University of California at San Diego*, 2004.

[39] L. Summerer, "Solar Power Satellites - European Approach", *ESA Advancet Concept Team*, 2003.

[40] N. Takeichi, H. Ueno, M. Oda, "Feasibility study of a solar power satellite system configured by formation flying", *Acta Astronautica*, Vol. 57, pp. 698-706, 2005.

[41] URSI, *Report of the URSI Inter Commission*, June 2007.

[42] J.R. Wertz, *Spacecraft Attitude Determination and Control*, Kluwert Academic Publishers, Dordecht, 1978.

[43] B. Wie, *Space Vehicle Dynamics and Control*, AIAA Education Series, Washington DC, 1998.

[44] B. Wie, C. Roithmayr, "Integrated Orbit, Attitude and Structural Control System Design for Space Solar Power Satellites", *American Institute of Aeronautics and Astronautics - AIAA*, AIAA 2001-4273, 2001.

[45] B. Wie, C. Roithmayr, "Attitude and Orbit Control of a Very Large Geostationary Solar Power Satellite", *Journal of Guidance, Control and Dynamics*, Vol. 28, No. 3, pp. 439-451, May-June 2005.